2019

Design, Prototyping And Fabrication Of Powder Spray Device For Dehydrated Biological Particulates

James Reilly
University of Vermont

DESIGN, PROTOTYPING AND FABRICATION OF POWDER SPRAY DEVICE FOR DEHYDRATED BIOLOGICAL PARTICULATES

A Thesis Presented

by

James Reilly

to

The Faculty of the Graduate College

of

The University of Vermont

In Partial Fulfillment of the Requirements
for the Degree of Master of Science
Specializing in Mechanical Engineering

January, 2019

Defense Date: November, 7th 2018
Thesis Examination Committee:

Rachael A. Oldinski, Ph.D., Advisor
David M. Warshaw, Ph.D., Chairperson
Yves Dubief, Ph.D.
Niccolo Fiorentino, Ph.D.
Cynthia J. Forehand, Ph.D., Dean of the Graduate College

ABSTRACT

Tissue sealants of a liquid based formulation are widely studied in biomedical research with many starting to gain FDA approval. To date, little investigation has been put toward methods of application for tissue sealant materials, more specifically a powder based formulation. The focus of this research was to develop and prototype a powder spray device capable of administering powder based formulations with a long-term goal of integrating the device within the clinical setting. Powders can be administered in a variety of dry forms. These forms can range from non-homogenous nanoscale particles to homogeneous micro and nano-scale spheres. Incorporation of therapeutics within the powder makes this method of application favorable for the prevention or maintenance of disease. Pneumatic conveying is the transport of granulated solids using gas and is the principal basis from which the powder spray gun was designed. Fluidization aids were added to the device in order to increase powder flow properties. Analysis of spray field, spray rate, characterization of powder and ex-vivo testing was performed. All results suggest that the powder spray device is applicable for the deposition of powder based tissue sealants in a clinical setting.

TABLE OF CONTENTS

Page

LIST OF TABLES

LIST OF FIGURES

CHAPTER 1

CHAPTER 2

CHAPTER 3

CHAPTER 1: INTRODUCTION

1.1. Biologically Derived Medicinal Powders

The use of biologically compatible powders in the field of modern medicine is still in its infancy. Though the application of powder based materials for medicinal benefit is not new, the full capabilities of this mode of delivery have yet to be explored presenting a gap in the literature. Historically, plant based herbal medicines were often the only available source for indigenous and remote civilizations as they used only what the earth had to offer. These herbal concoctions can be processed into a variety of forms. In ancient Chinese society, these remedies were often delivered as a decoctionis, which was a water based formulation created by boiling medicinal agents from various plant types for an extended period of time. They can also be delivered in the form of a honey pill which combines powdered herbs with a concentrated decoction and honey to produce a pill like capsule for ingestion. In addition, these herbal remedies were consumed in their dried powder form demonstrating that powdered remedies have been in use for many years with success. [11]

The continued use of natural based herbal remedies remains a popular source of medicine today. According to the World Health Organization (WHO), traditional medicine accounts for nearly 40% of total health care delivered in countries such as the US, China and Columbia with this number trending upwards toward 70% in countries such as Canada and Chile [12]. A study conducted in Tamil Nadu, a southern district of India, suggests that many of the traditional medicinal concoctions are of powder form or contain some sort of powder additives. Figure 1.1a depicts the results of this study which show that 20% of traditional remedies are prepared in a powder formulation.

Though it is important to note that many pastes and decoctions include powder additives of some kind to give the paste additional medicinal benefits. As an example, the Gymnema sylvestre offers both a root powder and a leaf powder, used to treat poison bites and diabetes respectively. These powders are traditionally produced by grinding the plant in a mortar and pestle until the desired consistency is met. Other conditions commonly treated with traditional remedies range from topical wound healing to asthma and stomach conditions as seen in Figure 1.1b. [10]

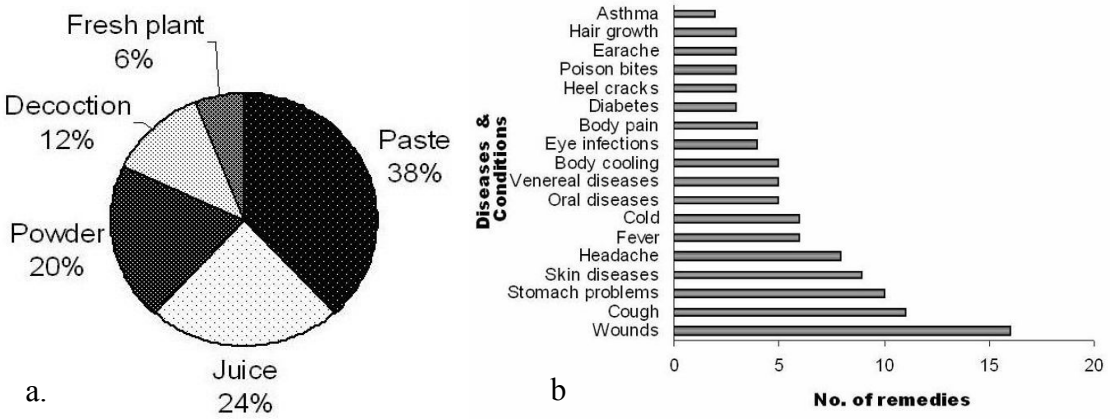

Figure 1.1. a) Methods of traditional herbal remedy preparation. b) Depicts a list of diseases and conditions that each have a number of remedies based on holistic treatments. [10]

In the modern medical setting, powder formulations are still being used for a wide variety of applications. Two common conditions treated with the use of powder based materials include internal hemorrhaging and asthma. Both disorders mentioned can be alleviated with the use of a powder based treatment. The application of a powder formulated therapeutic often requires a unique method for treatment delivery which must be carefully designed with the target tissue sight in mind. For the mitigation of

internal hemorrhaging an endoscopic delivery system is required in order to deposit the treatment within the gastrointestinal tract with minimal invasive action. To administer treatment for individuals suffering from asthma a specially designed dry powder inhaler (DPI) is used in conjunction with extremely fine powders in order to ensure dosage reaches the smaller branches of the bronchial tree.

Gastrointestinal bleeding (GI bleeding) is a frequent complication seen in the clinical setting that, if left untreated, could cause severe damage to a patients intestinal tract. Recently multiple powder based hemostatic formulations have been created for use in endoscopic procedures [13]. One hemostatic powder of interest is the Endoclot Polysaccharide Hemostatic System (PHS). This engineered system is designed to work in unison with the working channel of an endoscope. Endoclot Absorbable Modified Polymer (AMP) is a unique powder formulation from a modified starch derivative that acts as the hemostatic powder of Endoclot PHS. This compound is a biocompatible and absorbable hemostatic agent which gels upon interaction with water molecules in and around the bleeding wound sight. The complete system includes both the dehydrated powder formulation AMP as well as the mechanism for its delivery. In the case of Endoclot PHS, the delivery mechanism consists of a catheter like tubing system that is connected to an air compressor via a Y connector, as seen in Figure 1.2a. The powder is contained within an applicator which consists of a powder mixing chamber that is manually agitated to encourage the deposition of powder into the air stream and then through the working channel of an endoscope to the target tissue sight. This technique

is used to treat issues such as peptic ulcer bleeding or bleeding from minimally invasive surgery. [14]

a. b.

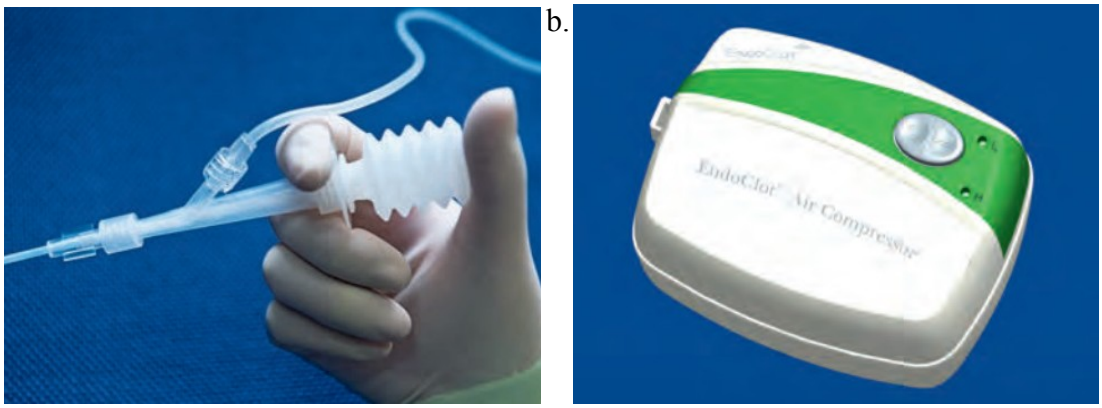

Figure 1.2. a) Endoclot applicator containing AMP powder formulation. Tapping of the applicator agitates powder and initiates the flow through the catheter tubing. b) Compressor that provides the air to propel powders through working channel of the endoscope at a pressure hovering around 2 PSI. [endoclot.com]

The inhaler class of medicine delivery is another example where dry powder is utilized within the clinical setting. The objective of a DPI is to administer doses directly to a patient's lower respiratory tract and maximize the amount of drug that is delivered to the target tissue sight. Dry powder inhalers (DPI) make up a large class of devices that are used to help individuals suffering from a variety of complications. The interior pleural membrane is a favorable site for the uptake of drugs because the environment in the lung is not nearly as harsh as that of the gastrointestinal tract. Many unique DPI designs have been applied to medicating the lung [15, 16].

1.2. Alginate Based Tissue Sealants

Research conducted in the Engineering Biomaterials Research Laboratory (EBRL) at UVM has shown chemically modified alginate to be a promising liquid tissue sealant for pleural air leaks, demonstrating similar burst pressure to some leading existing liquid sealants [17, 18]. The significance of this material relates to the innate non-toxicity in combination with biocompatibility. This is in part due to the fact that alginate is a natural derivative extracted from brown seaweed. As a source based in nature, alginate is naturally abundant and cheap to process making alginate based tissue sealants an extremely attractive class of materials within the biomedical industry.

In a powder form, the alginate readily hydrates upon application to a wet tissue site. During hydration of the applied powder formulation, the wound site will experience a period of dryness which is favorable to promote sealant adhesion and prevent the washing away of material due to continuous flow wound exudate.

Once applied, the material will provide an immediate defensive coating capable of maintaining a moist environment to stimulate the natural healing process. With the addition of a crosslinking mechanism, alginate can then form a hydrogel network which has the ability to adhere to local tissue while maintaining a hydrogel structure. This characteristic provides a functional basis that sequentially enables a wide variety of possible applications.

1.2.1. Chemical Modification of Alginate

Alginate is a naturally occurring polysaccharide extracted from brown seaweed [9]. The extraction process is intended to convert alginate into a soluble form of sodium alginate which can then be incorporated with a multitude of potential consumer applications [9, 19]. On a molecular scale, the alginate polymer is more specifically a binary copolymer, consisting of (1-4) linked β-D-mannuronic acid (M) and α-L-guluronic acid (G) monomers [9]. The block structure of alginate can be seen in Figure 1.3, and it is important to note this block structure is not necessarily the same in all samples.

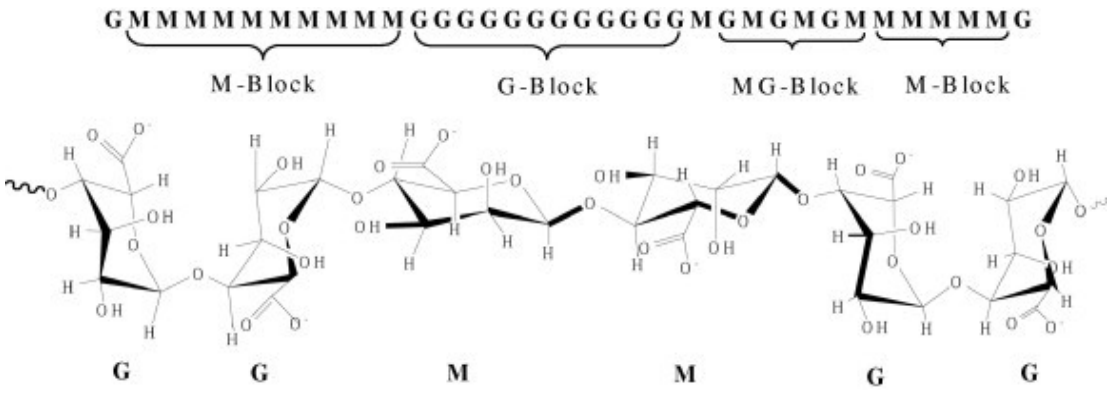

Figure 1.3. Block structure of alginate showing the repeating G and M block combinations. [9]

Sodium alginate, when in solution, has the ability to readily form strong hydrogels via ion exchange between divalent or multivalent cations, such as Ca2+. This occurs when the calcium ion is highly coordinated to hydroxyl and carboxylate functional groups of four G monomers from two neighboring polymer chains. [20]

Sodium alginate has a lot of idle carboxyl and hydroxyl groups which leaves the possibility for further functionalization by use of chemical reactions. Methacrylated alginate is a functionalized polymer produced via esterification of alginate hydroxyl

groups with methacrylic anhydride or glycidyl methacrylate, and can undergo rapid polymerization in the presence of UV light to enable covalent crosslinking of the alginate network [20]. To avoid the use of UV light, alginate can be covalently crosslinked with visible green light Eosin Y, triethanolamine, and 1-vinyl-2-pyrrolidinone as the photo- sensitizer, photo-initiator, and catalyst respectfully [17]. These chemical characteristics of sodium alginate enable functionalization to promote an increase in utility of the material.

1.3 Dilute-Phase Conveying Systems

There are numerous methods to transport materials using pneumatic conveying. "A pneumatic conveying system is a process by which bulk materials of almost any type are transferred or injected using a gas flow as the conveying medium from one or more sources to one or more destinations" [4]. This method of solid transport is attractive because it offers multiple advantages. These systems are cost-effective and they completely encircle the solid being transported while keeping material from coming into direct contact with moving mechanical parts. Another advantage of pneumatic conveying systems deals with the versatility they allow. It is relatively easy to reroute or add on to this type of transport system which makes it a good choice for any growing operation. Typically, air is used as the gas medium unless there is a risk for explosion or fire which oxygen would accelerate.

There are three general methods applied to pneumatic transport conveying systems. These methods include dilute-phase conveying, dense-phase conveying and air-activated gravity conveying. Dilute-phase conveying is a continuous process which includes either pushing or pulling of materials by means of large air velocity and low pressure. Dense- phase conveying utilizes a pulse of air to push a slug of material along by means of high pressure and low velocity. Air-activated conveying simply conveys material on top of a cushion of air. Among these various systems, the dilute-phase conveying is of particular interest for application in small scale biomedical dehydrated particulate handling. [4]

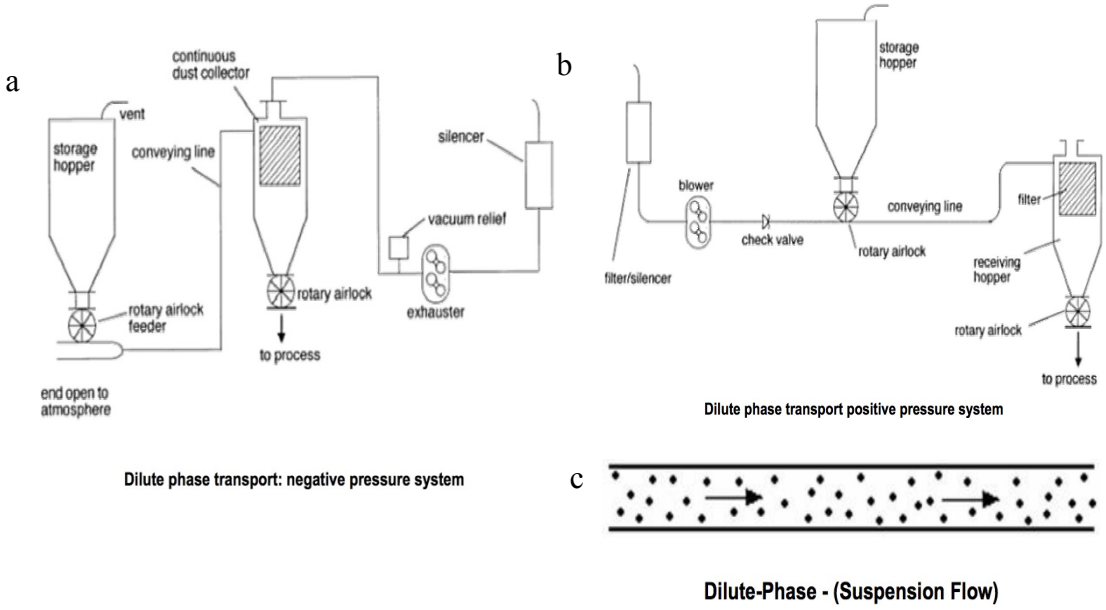

Figure 1.4. a) Dilute-phase negative pressure utilizing vacuum forces to facilitate the transport of material. b) Dilute-phase positive pressure utilizing a blower to generate air flow and transport material. c) Example of what dilute-phase conveying looks like as particulate is suspended in the moving air stream. [4]

Dilute-phase conveying is a sub set of pneumatic transport systems in which material is distributed as a suspension in the gas used as the conveying medium, see Figure 1.4c. In general, there are two main categories of dilute-phase conveying, positive pressure conveying systems and negative pressure conveying systems, see Figure 1.4a and Figure 1.5b. In both system designs, powder originates in the storage hopper which then feeds material to the conveying line. These storage hoppers utilize the ever-present force of gravity to naturally guide material towards the exit chute of the hopper.

To modulate or control the release of material from the hopper into the conveying line, there are two mechanisms commonly used, the venturi feeder and the rotary valve feeder, see Figure 1.5a and Figure 1.5b. Venturi feeders are an attractive component because they do not have any moving parts. The material flows through the

hopper via gravity and then enters the moving air stream as a function of the fluid velocity. The venturi effect is a well-known principle of incompressible fluids where there is a reduction in fluid pressure accompanied with an increase in fluid velocity through a constricted or choked section of pipe. This is a result of energy and mass conservation. Since there are no moving parts, venturi feeders do not require maintenance or complex controls. The down side is that they must be catered for a specific powder and sometimes experience blockage if there is any significant variation in system operation. Rotary feeders are of interest because they can easily modulate and control the amount of powder introduced into the air stream. Due to their complexity, increased controls and maintenance are required in order to maintain smooth operating conditions. Some issues with the rotary feeder systems include inadequate feed rate, wear, and leakage. Over time, components will experience wear which, in some cases, can cause material to leak through altering the feed rate. [3, 4]

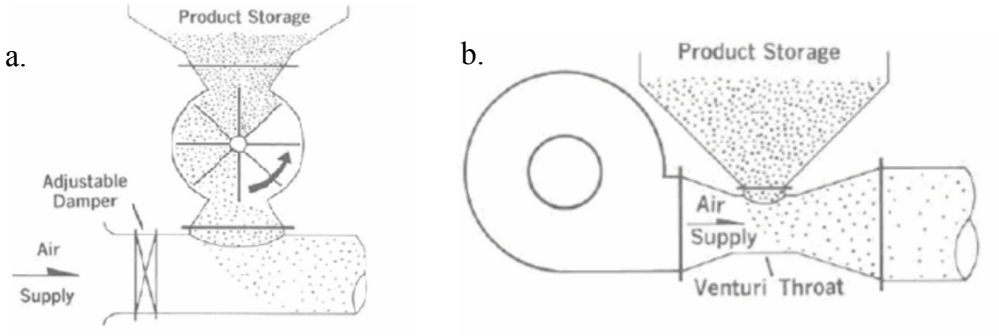

Figure 1.5. a) Sample schematic for a rotary valve feeder. b) Sample schematic for a venture feeder. [4]

1.3.1. Characterization of Particles

Utilizing the flow of a pressurized gas to accelerate dry powder particulates has been applied to a variety of processes. From pneumatic conveying to surface finishing, the transport of solid particulates has use in many industries. Unlike fluids, solid particulates are difficult to convey and transport. This can be attributed to the complexity surrounding their physical particle interactions as well as their material surface properties and how these manifest when a material is being handled in bulk. Many of these interactions can vary widely amongst a diverse group of powders. This variety of characteristics requires a particular set of operating conditions when designing a transport system. If not engineered correctly there is a high likelihood the system will experience particle agglomeration, cohesive arches and funnel flow, all of which will impede the flow of powders and interfere with system operation. To avoid these scenarios, pneumatic transport systems are typically engineered for conveying a specific powder type as part of a larger operation.

The dispersion of powder in an air stream is dependent on a multitude of factors. In general, some of the most influential factors being particle size, particle shape, and inter-particle adhesion forces. It is important to first characterize particles on a localized scale to obtain insight towards what conditions are required to best handle that specific type of powder. Furthermore, many of these seemingly micro scaled characteristics can be related to how a powder behaves when in bulk form. Bulk properties of a powder help to better understand and predict the behavior of that powder as it is dynamically handled. It is important to recognize the conditions that best illicit powder flow when designing a system to facilitate this process.

Individual particle geometry is a factor that influences macroscale behavior of that material in bulk form. Since it is rare that a powder formulation is composed of uniform spherical particles, often reference parameters are used for geometric description. Volume diameter, d_v, is defined as the diameter of a sphere having the same volume as the particle of interest and can be described with equation 1.1. [3]

$$d_v = \left(\frac{6V_p}{\pi}\right)^{\frac{1}{3}} \qquad \rightarrow \qquad V_p = Volume\ of\ Particle \tag{1.1}$$

Along with volume diameter, surface diameter d_s, describes a sphere with diameter the same as that of sphere with identical surface area to the particle of interest. This mathematical expression can be seen in equation 1.2. [3]

$$d_s = \left(\frac{S_p}{\pi}\right)^{\frac{1}{2}} \qquad \rightarrow \qquad S_p = Surface\ Area\ of\ Particle \tag{1.2}$$

Combining the two concepts seen in equations 1.1 and 1.2, equation 1.3 describes what is called the surface-volume diameter. This metric is expressed as the diameter of a sphere having equal external surface area to volume ratio as the particle of interest. Particle density, ρ_p, is described with equation 1.4. [3]

$$d_{sv} = \frac{6V_p}{S_p} = \frac{d_v^3}{d_s^2} \tag{1.3}$$

$$\rho_p = \frac{Mass\ of\ the\ particle}{\begin{array}{c}Volume\ that\ particle\ would \\ displace\ if\ its\ surface\ was\ non-pourus\end{array}} = \frac{M_p}{V_p} \tag{1.4}$$

Furthermore, the above equations can be combined to form an expression to describe the shape factor of a given particle. Sphericity, ϕ, was first introduced by Hakon Wadell in 1933 as a means to relate non-spherical particles to that of their strictly spherical counterpart [21]. A perfectly spherical particle will have a sphericity

equal to 1. The mathematical representation of this factor can be seen in equation 1.5. [11]

$$\phi = \frac{Surface\ Area\ of\ Volume{-}Equivalent\ Sphere}{Surface\ Area\ of\ Particle} = \left(\frac{d_v}{d_s}\right)^2 = \frac{d_{sv}}{d_n} \tag{1.5}$$

Although defining equations 1.1 through 1.4 as factors that describe a particles geometry helps to relate irregular particle shapes to that of a simple uniform sphere, this information alone is not sufficient to make predictions about a powders flowability. To do this, more information must be taken into consideration.

Describing particle behavior with fluid dynamics allows for calculations that predict limiting flow conditions such as the terminal velocity of a particle. Before this can be calculated, some basic fluid dynamic parameters must be introduced. The force acting on a single particle suspended in flow can be depicted using equation 1.6. This equation can be rewritten and solved for the coefficient of drag, C_D, shown in equation 1.7. For these equations ρ_f is the fluid density (kg/m3), Ur is the relative velocity between the particle and the fluid, and A_p is the area of the particle (m2). To obtain velocity of the particle, a slip factor is often employed. For most solids, the slip factor is .8, which means that the particle is traveling at roughly 80% of the gas velocity. [3, 4]

$$F = \frac{1}{2} C_D \rho_f U_r^2 A_p \tag{1.6}$$

$$C_D = \frac{F}{\left(\frac{1}{2}\rho_f U_r^2 A_p\right)} \tag{1.7}$$

The drag coefficient is also dependent on the particle Reynold's number, Re_p, equation 1.8. Here μ (kg/m*s) is the fluid viscosity.

$$Re_p = \frac{U_r d_p \rho_f}{\mu} \tag{1.8}$$

Once the coefficient of drag and the Reynolds number are identified the terminal velocity of a spherical particle can be predicted. To make this prediction, first a dimensionless value describing particle size, d_p^*, must be found, equation 1.9. Once this has been accomplished, the terminal velocity of a particle can be solved for using the second equation seen in equation 1.10. Assuming that the sphericity of the particle is equal to 1, the terminal velocity can be quickly solved for using the first equation expressed in 1.10. [3]

$$d_p^* = d_p \left[\frac{\rho_f(\rho_p - \rho_f)g}{\mu^2}\right]^{\frac{1}{3}} = \frac{3}{4}\left[C_D Re_p^2\right]^{\frac{1}{3}} \tag{1.9}$$

$$U_t^* = \left[\frac{18}{d_p^2} + \frac{.591}{d_p^{*\frac{1}{2}}}\right] = \frac{4}{3}\left[\frac{d_p(\rho_p - \rho_f)}{\rho_f C_D}\right] \tag{1.10}$$

Other parameters that can prove helpful when determining a powders flowability include angle of repose and the angle of internal friction. Flowability is defined as the ease with which a bulk material flows under the influence of gravity only [4]. These measures offer practical importance as they do not depend on any theoretical assumptions. Figure 1.6 illustrates how these parameters can be determined experimentally. Typically, a smaller angle of repose suggests that material has a higher flowability. Values for angle of repose that are associated with materials who demonstrate favorable flowability are within 30° → 40°. Similarly, in order for a

powder to flow, the angle of internal friction, β, must be greater than the angle of repose, α. [2-4, 22]

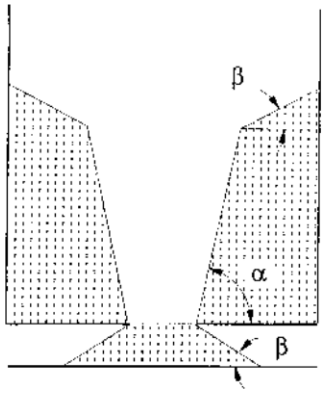

Figure 1.6. Experimental set up for determining angle of repose (α) and angle of internal friction (β). [3]

To predict when a material will initiate flow, threshold shear stresses must be examined and understood. A theory has been developed by A. W. Jenike which can be used to determine the hopper slope required to facilitate the desired mass flow of a bulk powder. During mass flow, all material contained in the hopper is in motion allowing for a continuous discharge, Figure 1.7.

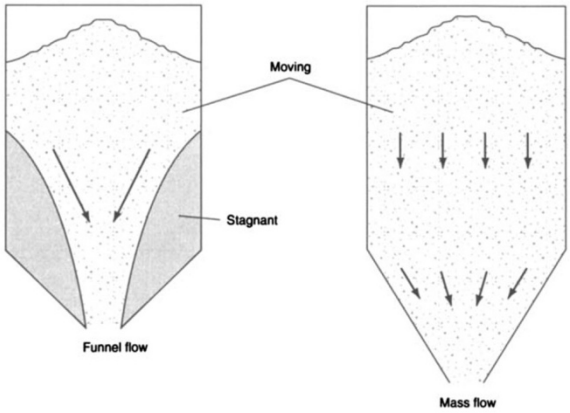

Figure 1.7. Two main flow types that can occur within a hopper. [2]

Jenike's theory involves finding the Yield Limit (YL) which is the curve tangent to all Mohr's circles that represent the onset of flow, Figure 1.8. The values for consolidation stress (σ_1) and unconfined yield stress (σ_c) are collected experimentally using a rheometer equipped with powder shear testing capabilities.

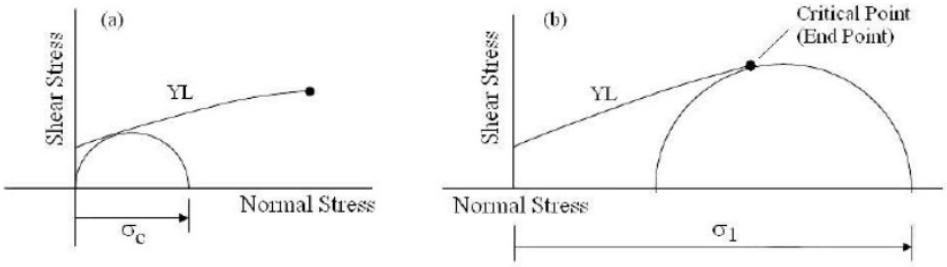

Figure 1.8. Mohr circles for a) unconfined yield stress and b) consolidation stress or compacting stress. [6]

This test can be conducted multiple times using a variety of consolidation states. In return, a set, including corresponding σ_1 and σ_c values, is collected for each consolidation state. These $\sigma 1$ and σ_c pairs can then be plotted together, and the line connecting them is known as the flow function (FF), Figure 1.9.

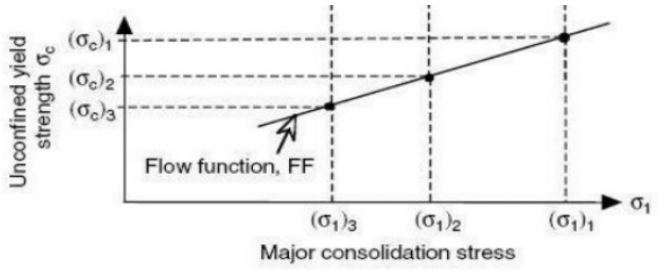

Figure 1.9. Flow Function (FF) defined as a function of σ_1 and σ_c pairs. [6]

The slope of a FF can be used to approximate the flowability of a powder. Decreasing values of slope suggest a material that exhibits higher flowability than one

with a larger slope, Figure 1.10. The inverse of FF is known as the flow index (ffc) which is an easy way to classify a powders flowability. The larger ffc, the more likely a material is to flow. A ffc below 4 suggests a material is cohesive or hardened, while values above 4 suggest a material is easily flowing or even free flowing. [7]

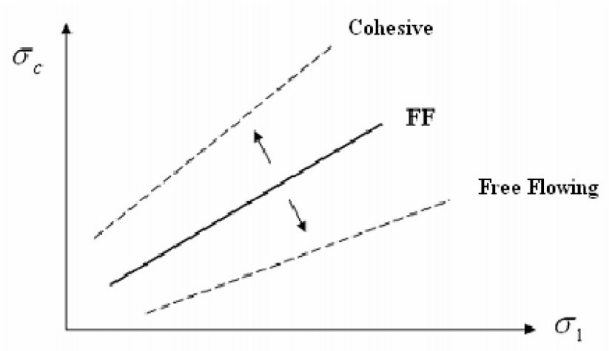

Figure 1.10. Flow function (FF) graphical visualization on the flowability of a material. [7]

Up until this point, many tests have only been able to give a general inclination as to the flowability of a powder based on some mechanical characteristics. However, using Jenike's theory, the minimum outlet diameter for a hopper can be determined mathematically. To accomplish this, it is necessary to first define a hopper's flow factor (ff), equation 1.11. Flow factor (ff) is a function of consolidation stress ($\sigma 1$) and the stress necessary to support a stable bulk solid arch ($\bar{\sigma}_1$)[6].

$$ff = \frac{\sigma_1}{\bar{\sigma}_1} \tag{1.11}$$

Once the flow factor (ff) has been established based on appropriate stresses, a line whose slope is equal to that of the inverse of ff can be plotted with its starting point

at the origin. This line can be compared to the flow function (FF), Figure 1.11, and the intersection of these two lines is defined as the critical stress, σ_{crit}. [6]

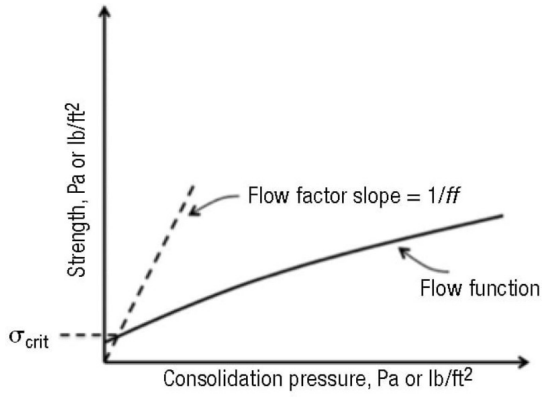

Figure 1.11. Intersection between flow function (FF) and flow factor (ff) gives the critical stress σ_{crit}. Beyond this stress, particle cohesion attractions are overcome. [5]

Once σ_{crit} is known, the minimum hopper outlet diameter, d_{crit}, can be solved for. This relationship is described with equation 1.12, where g is gravity and ρ_b is bulk density [6]. Not to be confused with the density of the material, the density of the powder, also referred to as bulk density, describes the ratio between apparent density of a powder and its tapped density. This diameter is a threshold value, any outlet diameter smaller than d_{crit} is susceptible to cohesive arching and flow interruptions.

$$d_{crit} = 2.2 \frac{\sigma_{crit}}{g \cdot \rho_b} \tag{1.12}$$

Apparent density (loose-poured density) of a powder is the amount of volume taken up by a loosely packed powder while the tapped density is the amount of volume occupied by a packed or tapped powder [2]. The apparent density of a powder will

always be less than the corresponding tapped density due to larger and more numerous voids being present. Figure 1.12 shows a collective relationship between apparent density and particle size which can be used to categorize powders with the type of pneumatic conveying system that will best facilitate the transport.

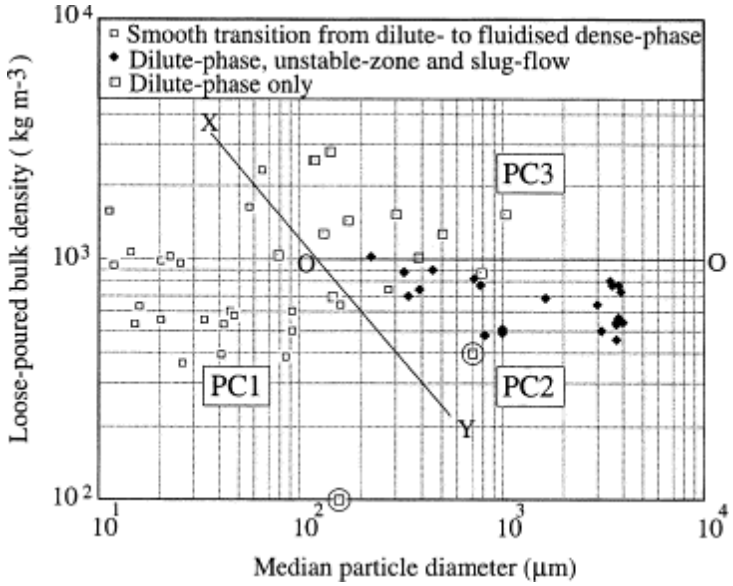

Figure 1.12. Loose-poured bulk density (apparent density) as a function of particle diameter to determine whether a powder can be handled in a dilute-phase or dilute/dense phase systems [8].

Methods for predicting flowability presented in this paper thus far all assume that the powder being handled does not change characteristics through time. This would suggest that properties such as moisture content and temperature remain constant without altering any characteristics of the powder in bulk form. In reality, changing these factors can have a large impact on the particle-particle interactions, which in turn changes the stresses required for a bulk powder to flow. Since it is extremely difficult for a system to completely isolate material from environmental influences, fluidization is employed as a means to minimize any of these effects.

Merriam-Webster dictionary defines fluidize as, to cause to flow like a fluid. In an industrial setting the most common source of fluidization comes in the form of bubbling a gas (usually air) through a powder in a particular manor to overcome inter-particular attractions that inhibit flowability. A substitute method for inducing fluidization comes when a source of vibration is introduced. Vibration applied to the hopper of material will introduce energy to the bulk powder promoting deagglomeration if the energy applied is larger than the cohesion forces between particles within the powder. A critical vibrational amplitude exists for each individual powder formulation beyond which the powder will experience instability [23]. This suggests that vibrational fluidization can be used to aid in flow properties of a powder.

CHAPTER 2: METHODS

2.1. Preliminary Prototyping

In order to analyze the effectiveness of a material in dry powder formulation, a custom spray device must be developed and tested. This device must have the capability of spraying a controllable amount of material in a repeatable fashion. A simple and user friendly interface would enable this device to be used by individuals of a wide range of skills and knowledge. The design process followed during the progression of this prototype device is laid out during the rest of this section. The process outlines key decisions and components that were necessary for the success of device operation.

Initial stages of the design process involved development of multiple conceptual prototype variations. These conceptual design variations were compared to each other after a qualitative assessment was made to determine the prototype variation that offers the most versatility and simplicity while allowing for adequate control over key parameters. After deliberation, three general prototype variations were taken into consideration for further investigation; air driven, venturi driven and gravity fed designs. The decision to move forward with one of these designs is further discussed in section 3.1.

Before constructing a working prototype, it was important to understand what design constraints limit the physical layout of the device. The first thing to consider

when designing a powder spray device was how the powder will be stored and introduced to the system. A storage mechanism is needed, capable of isolating the powder from the surrounding environment during storage and easily introducing that powder to the spray device when necessary.

Another important aspect to consider before beginning the prototyping process was to decide how air will be introduced to the system. This is important because fittings and connectors will become a design constraint as they dictate what fixtures are needed to mate the air source and the spray device. The source of air is an important component that will be a factor in determining performance and control. Things to consider include user control of air pressure, the quality of the air, and continuous air flow. Similarly, a trigger mechanism was required in order to obtain user control of the air release. This trigger must work in unison with other features on the gun for proper functional integration and device operation. The trigger mechanism is responsible for controlling the release of air as well as the electronic components of the spray device.

Once introduced to the system a powder is handled, transported, and eventually sprayed. This requires a custom component, containment hopper, capable of interfacing with the powder storage container as well as leading powder in the direction of the moving air stream. Optimally, this component will be easily removable and interchangeable. Furthermore, this component must be air tight as to not allow the escape of any air and must be able to incorporate small electronic motors. A means to more precisely control the release of powder is explored. This includes incorporating a

valve capable of controlling the deposition of powder at a continuous rate. A rotary style valve was investigated with multiple valve style geometries.

The addition of vibrational energy can be the deciding factor as to whether or not a powder will flow. The source of vibrational energy was important as it must be compact and durable. A simple geometry would allow for seamless integration. A low power consumption was important as this would allow for battery powered prototype.

To construct the prototype a multitude of processes were used. All custom pieces were designed using SolidWorks CAD software and then 3-D printed. The 3-D printer used was called the Dimension Elite, Figure 2.1, and offers the best quality print available from the UVM Fabrication Laboratory. The Dimension Elite is capable of printing a part that is 203x203x305mm. The layer thickness of the Dimension Elite is 0.178 mm, which is the reason why this machine was chosen over a MakerBot.

Figure 2.1. Dimension Elite 3-D printer, located in UVM Fabrication Laboratory. High quality complex prints are possible due to support material. Support is then dissolved away in a base bath.

Soldering was used to consolidate the electrical components within the shell of this spray device. All soldering was done at the safe solder station located in the UVM fabrication laboratory, Figure 2.2. This space includes fume extractors and a solder station. High tech silver bearing solder was used to reinforce connections.

Figure 2.2. Soldering station in UVM fabrication laboratory. Solder tip temperature can be controlled as well as tip geometry.

2.2. Chemically Modified Alginate Powder

2.2.1. ALG-GM

Glycidyl Methacrylate Alginate, ALG-GM, was synthesized through an aqueous based reaction. A 1% (w/v) solution was created by adding Manugel GMB alginate (LF 200 FMC Biopolymer) to deionized (DI) water. The solution was heated to 40 degrees Celsius to shorten the time it takes for alginate to go into solution. Once the alginate has dissolved, the solution underwent a nitrogen flush for approximately 10 minutes.

Glycidyl Methacrylate was added in excess to the alginate solution. The reaction is left to take place in an environment with pH of 10 and at 60 degrees Celsius. The hydroxyl group is more active at higher temperatures and an alkaline environment encourages the alginate hydroxyl functional group to attack the glycidyl methacrylate. The solution is to let react for 20 hours and is then precipitated in ethanol. After this process, the resulting material went on dialysis for 4 days before being frozen and lyophilized. Addition of salts (NaOH and KOH) was done by dissolving the ALG-GM into solution and introducing salts to the mixture before another round of lyophilization.

2.2.2. ALG-GM

Methacrylic anhydride alginate, ALG-MA, was synthesized through an aqueous based reaction. A 1% (w/v) solution was created by adding Protanal alginate (LF 200 FMC Biopolymer) to a deionized (DI) water and phosphate-buffered saline (PBS) solution. This solution was then reacted with a 20-molar excess of methacrylic anhydride (Sigma Aldrich). From here the solution was adjusted to a pH of 8.5 with 5N sodium hydroxide for six hours, then dialyzed in DI water for 5 days. The resulting solution was then frozen and lyophilized to yield the modified material. Addition of salts (NaOH and KOH) was done by dissolving the ALG-MA into solution and introducing salts to the mixture before another round of lyophilization.

2.3. Scanning Electron Microscopy

Imaging of powder particulates was conducted using scanning electron microscopy (SEM). University of Vermont has a microscopy imaging center (MIC) equipped with a JEOL 6060 scanning electron microscope, Figure 2.3. The JEOL 606 SEM was equipped with an energy dispersive X-ray microanalysis system from Oxford Instruments.

Figure 2.3. JEOL 6060 Scanning Electron Microscope, UVM Microscopy Imaging Center. [http://www.med.uvm.edu/mic/sem]

Imaging began with sample and stub preparation. This included making sure that the material to be imaged was completely dehydrated. For this experiment, all samples were of a dry powder formulation prior to stub preparation. They were lyophilized to ensure complete dehydration. After material was completely dehydrated preparation of the specimen sample mount can begin. The sample mount used was an aluminum disk with a diameter of 25 mm and a thickness of 5 mm. Material was introduced to this disk by means of double coated carbon conductive tape. Once the

material adhered to the carbon tape, the sample stub was ready for the sputter coating process.

UVM MIC has an EMS150RS ES sputter coater from Quorum Technologies used to prevent charging and increase the signal to noise ratio. To use this machine, the sample must be secured inside the vacuum chamber at a distance of roughly 5 cm from the closed chamber lid. Once secured, the vacuum generator can be turned on and the Argon tank can be opened. Select Au/Pd 60:40 profile and click run to carry out the remainder of the sputter coating process.

Now the sample can be added to the JEOL 6060 SEM. To accomplish this, first vent the chamber of the SEM. Place the specimen sample into the specimen holder and place inside the open SEM, make sure the working distance is roughly 15 mm. Once sample is held securely within the SEM, evacuate the air and wait for chamber to reach vacuum.

The computer should be set to 15-20 KV with a spot size of 35. From here, the level of magnification can be adjusted along with the focus and contrast settings. These settings are tuned for a specific image and can be altered for desired picture appearance.

2.4. Proton Nuclear Magnetic Resonance Spectroscopy

Chemical modifications were confirmed using proton nuclear magnetic resonance spectroscopy (NMR). The University of Vermont Department of Chemistry has a Bruker Avance III HD 500 MHz 1H-NMR spectrometer which was used for the duration of this project, Figure 2.4.

Samples were prepared prior to use in the 1H-NMR spectrometer. To accomplish this, a solution was made containing the material of interest and D2O. Typically, 5 to 25 mg of material is used and dissolved in roughly 0.5 ml of D2O. This solution was then transferred to a NMR glass tube. Once the solution was in the NMR tube, it was introduced to the Bruker for data collection.

The software used to facilitate the Bruker's operation is called TopSpin. In this software, 1H 1D spectrum of the solution was analyzed at 20 Hz choosing D2O as a solvent with 16 scans.

Figure 2.4. UVM ^{1}H-NMR Bruker Avance III HD used to characterize and confirm chemical modifications.

2.5. Powder Manufacturing

Some processing was required in order to transform material that comes off the lyophilizer into powder. When a material was removed from the lyophilizer, the resulting material state closely resembles that of cotton candy. In order to generate a powder, the traditional process of grinding material into a powder by means of mortar and pestle, Figure 2.5, was used and combined with liquid nitrogen. After the material is lyophilized liquid nitrogen was introduced, that freezes the material and behaves more brittle. This brittle behavior allows for the mortar and pestle to grind the material into a powder form.

Figure 2.5. Mortar and pestle used to create powder formulation.

2.6. Spray Data

2.6.1. Spray Field

The spray field of the powder spray device was investigated as a function of distance. For the scope of this project, spray field was defined as the diameter of powder deposition as a result of spraying perpendicular onto a collection surface. For this experiment laboratory benchtop paper was used, Figure 2.6. The diameter was measured and an average was generated over multiple tests.

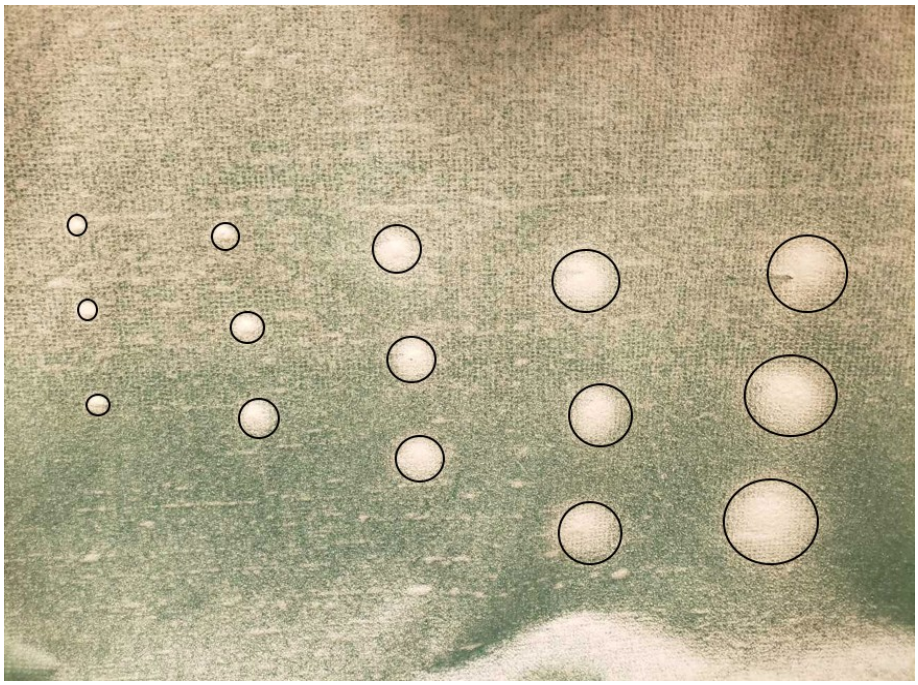

Figure 2.6. Spray field data collection schematic with superimposed boarders for impact diameter visualization.

This experiment was set up in a fume hood to prevent particulates from posing a possible hazard. The laboratory benchtop paper was hung vertically against the back wall of the fume hood. After this was done, the paper was coated in DI water so that the surface of the paper was completely sodden. The spray device was now held at the desired spray distance and aimed perpendicular to the benchtop paper. This was repeated a total of three times for each powder type at each spray distance. Data was collected at a spray distance of 1,3,6,9, and 12 cm from impact surface. The spray device was discharged until enough powder is deposited on the benchtop paper to clearly identify the boundary of the spray field. This was done visually as it becomes clear when this boundary can be clearly distinguished. Data averages were recorded and graphed to compare results between different powder types.

2.6.2. Spray Rate

The spray field of the powder spray device was investigated as a function of distance. For the scope of this project, spray field was defined as the diameter of powder deposition as a result of spraying perpendicular onto a collection surface. For this experiment laboratory benchtop paper was used, Figure 2.6. The diameter was measured and an average was generated over multiple tests.

The spray rate was defined as the mass of powder leaving the powder spray device per unit time. To gather this data in the laboratory setting, anti-static plastic bags were used, Figure 2.7. This was to prevent any latent static charge on the material from hindering the data collection process as normal zip-lock bags could actively repel statically charged powders and interfere with the data collection process.

Figure 2.7. Anti-static plastic bags used during the spray rate data collection process.

To collect data, the spray device was loaded with the powder of interest and set to the desired system pressure. Anti-static bags were then labeled with the class of material chute being used, amount of time being sprayed, pressure of the spray device, and what material was being sprayed. The spray times were collected at 1,2,3,6,9, and 12 seconds of continuous spraying (n=3). Once labeled, each bag was weighed and that initial weight was tabulated for all samples.

In a fume hood, the spray device was held at a distance of 5 cm away from an opened anti-static bag. The spray device was then fired into the anti-static bag for the duration that is indicated on the bag label. Once this has been done for all bags at all time points, each bag was weighed again and the results of this are tabulated. The difference between the bag with material and the same bag with no powder is the amount of material dispensed during the indicated spray duration. The amount of

material dispensed during a specific spray duration was then averaged between trials and tabulated along with standard deviations.

2.7. Angle of Repose

Determining angle of repose was done in lab using a standard plastic laboratory funnel and weigh boats. The funnel was fastened above a flat surface, on that surface an upside-down weigh boat was positioned directly under the funnel neck. The weigh boat was used because of the circular surface when placed upside down. This circular surface was needed because it allowed for each pile of powder formed to have the same base diameter. The only variable between powders was the height of the pile. This method was scaled down and modified form of standard industry practice [24]. This was done so that angle of repose can be determined using the limited amount of powder available for testing. The testing setup can be seen in Figure 2.8. To conduct testing, powder of interest was slowly introduced to the funnel as to avoid inertial forces hitting the pile. Testing was complete once the pile begins to flow over the side of the weigh boat. At this point the height of the pile was measured using a dial micrometer and tabulated, the testing area was cleaned and reset to collect angle of repose for the next powder sample.

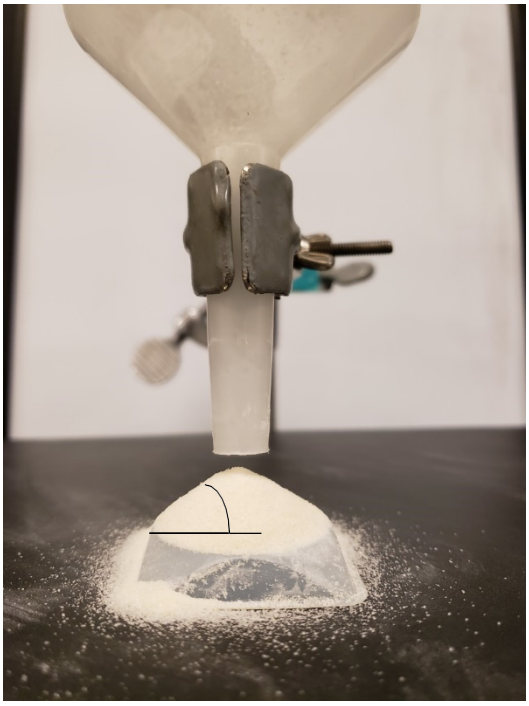

Figure 2.8. Laboratory setup for collection of angle of repose. Constant diameter weigh boat offers standard base diameter during testing to increase accuracy of results.

2.8. Burst Pressure

Testing burst pressure of chemically modified alginate was accomplished using a custom in house burst pressure device. Burst pressure testing included introducing an increasing pressure gradient to one side of a crosslinked hydrogel plug and recording the increase in pressure. This pressure increase was recorded until the hydrogel plug failed and the maximum pressure tolerated was considered to be the burst pressure. This testing device was previously developed as a masters project by Patrick Charron M.S of the EBRL at UVM [25]. The device, Figure 2.9, included a syringe pump and a pressure transducer connected to a chamber for testing the burst pressure of tissue sealants. The chamber and pressure transducer were housed within a temperature controlled incubator in order to prevent material not only from drying out during testing but to mimic physiological conditions.

Figure 2.9. Custom designed burst pressure device including syringe pump used to introduce air to test chamber.

Material groups for burst pressure testing included a control ALG-MA (non-powder) and the experimental group ALG-MA+Salt (powder) in liquid form, see section 3.4. Triethanolamine (TEOA) and Eosin y in vinylpyrrolidone (1VP) are added to the solutions of ALG-MA to enable photo-crosslinking with visible green light. Once the solutions are prepped, a wet collagen casing is punctured using a 3mm biopsy punch. The wet collagen casing is then sandwiched between a glass slide and a Teflon® mold, Figure 2.10. The material solution was added to the Teflon® mold which was centered over the hole previously made in the collagen casing. From here, the mold and material were exposed to green light for 10 minutes to initiate crosslinking. After this, the Teflon® mold and glass slide were removed and the collagen casing with the crosslinked ALG-MA hydrogel was secured inside the burst pressure chamber.

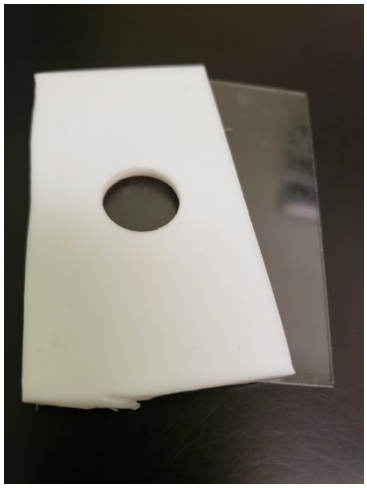

Figure 2.10. Teflon® mold and glass slide for burst pressure hydrogel plug formation.

Using Harvard Apparatus syringe pump software, pressure and time data sets were collected. Once data collection was initiated, the syringe pump is activated. The resulting data was then collected up to the point of hydrogel failure, data was then tabulated and saved for analysis.

2.9. Efficacy of Clinical Applications

An ex-vivo experiment was conducted to test the clinical efficacy of the powder spray gun design using a porcine heart (graciously donated by Dr. Jeffrey Spees). This experimental setup was designed to demonstrate that an injured tissue was capable of being coated in powder and then, once absorbed by the superficial fluid found on the tissue, crosslinked to form a hydrogel blanket to protect the damaged tissue sight.

Testing was conducted in a biosafety cabinet that was sterilized with UV light. The recently dissected heart was placed in a large petri dish. The powder spray device was then loaded with alginate powder which was then sprayed onto the heart at 20 psi from a distance of 6 cm. The alginate powder was then crosslinked with a calcium chloride solution. An overall qualitative assessment was then made on the performance of the spray gun and sealant to see how they can be implemented in the clinical setting.

CHAPTER 3: RESULTS

3.1. Final Prototype

3.1.1. Conceptual Prototypes

Three main prototype variations were developed and quantitatively compared. Positive and negative attributes of each design variation are considered. One of the three design variations was then chosen and used as the baseline for the duration of the design process.

The air driven conceptual prototypes rely on a constant stream of low velocity air to transport powder. This simplistic design has a single entrance and exit with no moving or electronic parts. Air was introduced to the system at a constant rate as seen in Figure 3.1. Following the path of least resistance, air was forced to leave through the only outlet which feeds into atmospheric conditions. Here, the interaction between moving air and the resting powder formulation was what provoked powder suspension in air. Although this design might be simple and without any complex moving parts, there was limited control with respect to the ability to regulate the amount of powder being introduced to the air stream. Similarly, material characteristics of the powder as well as the amount of powder present within the containment area significantly affect the operational conditions.

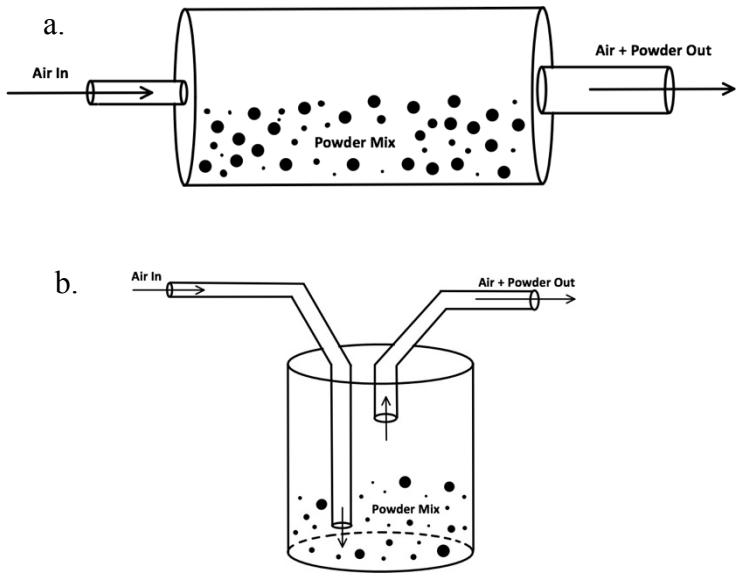

Figure 3.1. Conceptual prototype of air driven system, a and b.

Venturi driven design operates using a well-known principle of fluid dynamics known as the venturi effect. Shown in Figure 3.2, this generic design requires an air stream velocity that was sufficiently large enough to induce a significant venturi effect. The effect must have enough influence that the powder is effectively sucked into the air stream as a result of high air velocities. The air and powder mixture will exit to atmospheric conditions. This design consists of no complex moving parts and was dependent on the high velocity air stream to induce a venturi effect great enough to overcome the stagnant powder. Similar to the air driven design, material properties of the powder will limit operating conditions as well as control. Furthermore, the high velocity required to induce venturi effect could damage or irritate tissue upon impact.

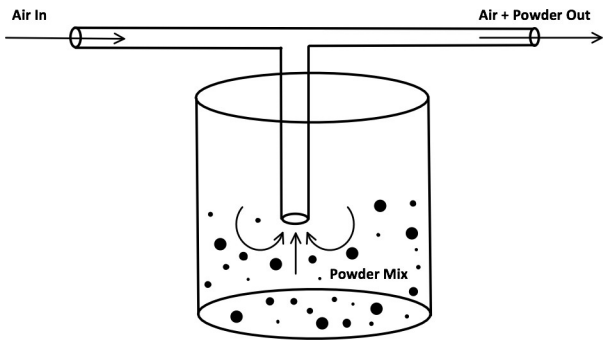

Figure 3.2. Conceptual prototype venturi design.

The gravity fed design was oriented in such a way where the powder formulation was contained above the air stream leaving a gravitational potential difference between the two. This design can be visualized in Figure 3.3. The gravity fed design requires the integration of electronic controls to add an increased level of control over system parameters. This design included the utilization of vibrational motors to excite the powder and disrupt any inter-particle cohesion that may prevent steady flow. A media isolation valve, also known as a pinch valve, Figure 3.3, was used to regulate the feed rate of powder. There are various other ways to regulate the flow of powder. For example, a rotary valve style feeder could be employed or even no feeder at all.

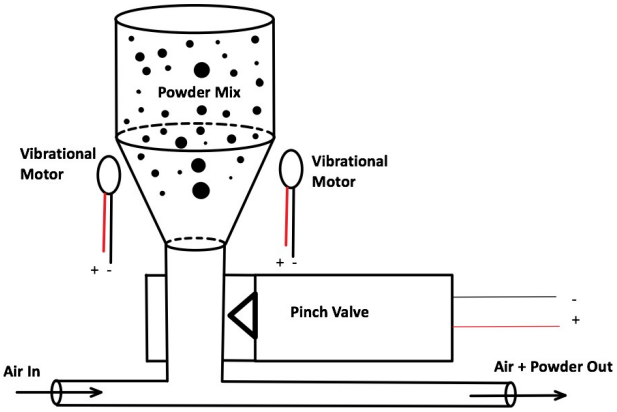

Figure 3.3. Conceptual prototype gravity fed design.

After a qualitative assessment of these preliminary conceptual designs, the decision was made to move forward with the gravity fed conceptual design. Here, the force of gravity was used as one feeding mechanism while the vibrational motors and feeder (pinch valve) help to facilitate this process. Though, the pinch valve was abandoned and replaced with a rotary valve and 360-Servo which is explained further in section 3.18. Now that the preliminary design of interest has been determined, prototyping can take place.

3.1.2. Particulate Storage Mechanism

As mentioned in section 2.1, the storage mechanism was a key design parameter. This was because customized fittings must be designed on the spray device that will attach to the storage mechanism in order to introduce powder to the system. This connection must be simple and easy for the user to achieve. For this spray device, a static dissipative plastic (SDP) container was chosen, Figure 3.4. It is important that the container had static dissipative properties in order to lessen the magnitude of any static charge present on the powder. Without a static dissipative container, static charge of particulates could inhibit the flow of that material and disrupt device function. This SDP container also had a snap on lid which can be easily mimicked and integrated with a custom designed connection interface.

Figure 3.4. Static dissipative plastic containers from ESD plastic containers. Snap lid design is allows for easy interfacing with custom components.

3.1.3. Containment Hopper

This SDP container must rigidly connect to the spray device to prevent air or material leakage which would result in a loss of pressure and device function. The custom piece designed to accommodate this was called the containment hopper. Initial design iterations focused on a hopper capable of 'snapping' to the storage mechanism. This was achieved by replicating the cap geometry in SolidWorks CAD software. Figure 3.5 depicts the first iteration of the containment hopper. Notice there are two design variations, one with an extruded insert for a rotary valve and the other without. Multiple components of each design were generated using a high resolution 3-D printer. The resulting part was a working ABS plastic model and the storage mechanism rigidly snaps onto the containment hopper as intended.

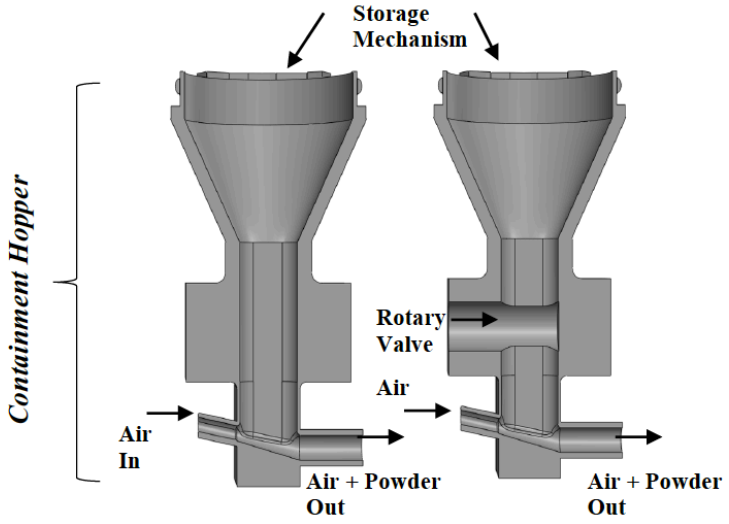

Figure 3.5. First iteration of containment hopper design. rotary valve (Left). Includes opening for rotary valve (Right).

After having a working model capable of interfacing with the storage mechanism, the next phase included designing an improved version of the previous model. In the updated model, exterior voids and gaps are filled in with material to give a more solid build while also bringing the air intake connection and moving it in line with the exit connection, Figure 3.6. Moving the air intake changes the path of air flow allowing powder and air to fill the mixing chamber before exiting the device. This critical change resulted in improved device performance. A rib is also added, seen above rotary valve, for easy integration with a device shell later in the design process.

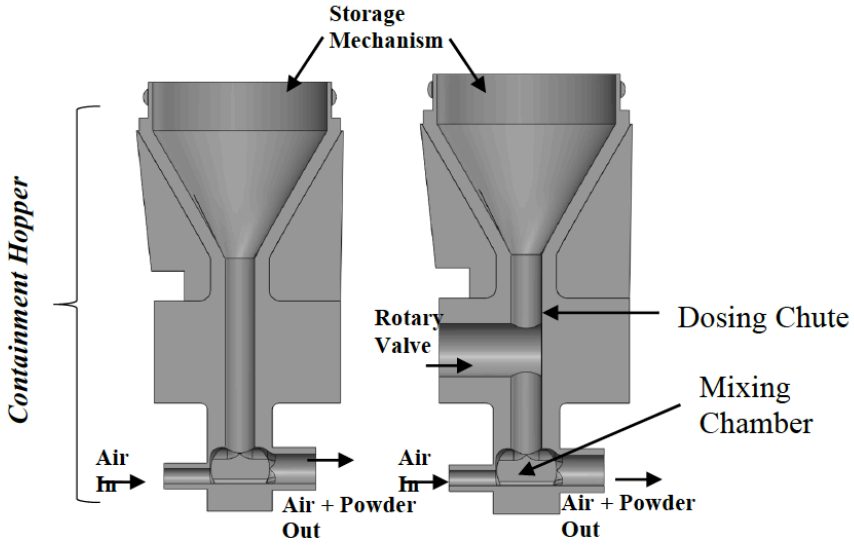

Figure 3.6. Final design of containment hopper. No rotary valve (Left). Includes opening for rotary valve (Right).

As stated earlier, there were two parallel designs including one with an extruded insert for a rotary valve and the other without. Similarly, there were two design variations that offered different dosing chute geometries. The dosing chute begins at the base of the funnel and ends at the mixing chamber as seen in Figure 3.6. The two

geometries investigated include a circular chute and an elliptical chute, Figure 3.7. A larger elliptical dosing chute was needed to handle powders with larger particle sizes whereas the smaller circular dosing chute might inhibit flow and even cause cohesive arches for such powders. For this reason, both geometries are applied in order to give the device a wide range of operation.

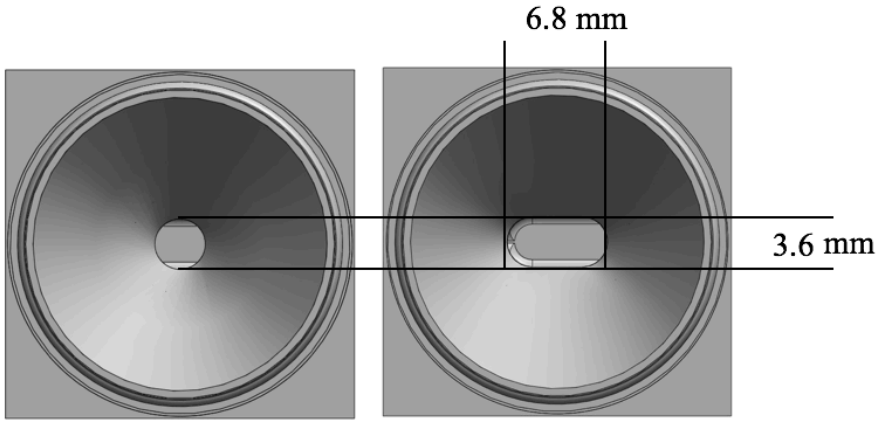

Figure 3.7. Circular dosing chute (Left) and elliptical dosing chute (Right).

Another feature added to the improved containment hopper design involves vibrational motor integration. Visualized in Figure 3.8, disk cutouts have been extruded from the exterior of the containment hopper. This allowed for the vibrational energy of the mini motors to effectively transfer to the powder as they are in close proximity to the interior of the funnel.

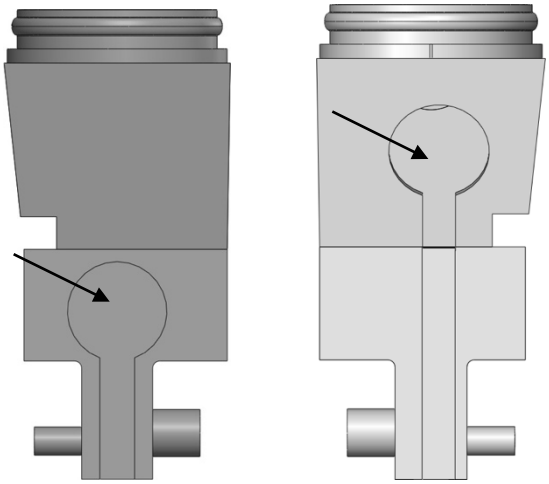

Figure 3.8. Vibrational motor disk cut out from containment hopper.

Using a 3-D printer for prototyping offers many advantages but can come at the cost of some material properties. The resulting 3-D printed ABS plastic was a near perfect model of the SolidWorks part drawing. Due to the layer deposition of the 3-D printing process, a printed model was left with a semi-porous structure. This porosity resulted in air leakage throughout the containment hopper during device operation. As a solution, multiple layers of a nail polish clear coat were applied to the exterior surface of the containment hopper. Clear coat soaked into the voids of the ABS containment hopper making it air tight.

3.1.4. Spray Gun Shell Design

For a compact device, all components must be consolidated internally within some sort of shell or housing. This exterior shell was important for ensuring the function of each component. Holding pieces in place will allow for them to behave as intended. The exterior shell for the powder spray device was designed and drafted using SolidWorks CAD software and then 3-D printed out of ABS plastic. A look at the complete shell exterior and interior can be seen in Figure 3.9.

The device shell was designed with a lip and groove fastening mechanism that follows the boarder of the spit line which goes though the center of the shell. This lip and groove enables the device shell to snap together and pull apart. This allows for custom parts such as the containment hopper to be easily switched out during testing.

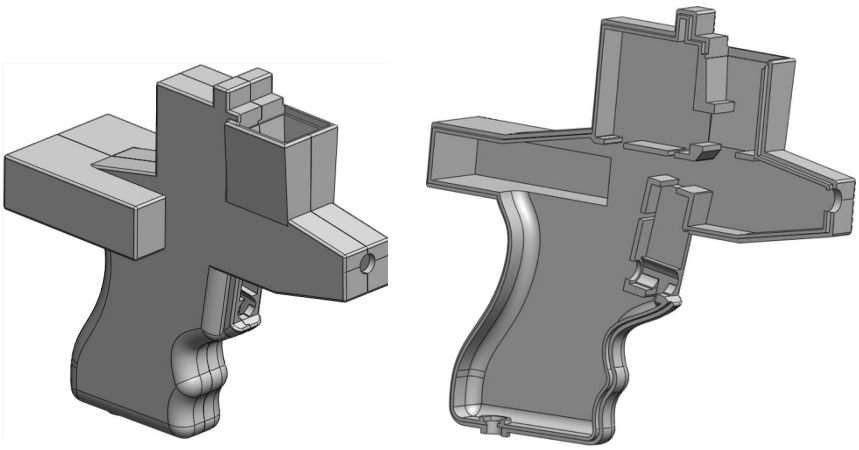

Figure 3.9. Complete powder spray device shell (Left). Half of device shell depicting internal section layout (Right)

Each section within the interior of the shell has been dimensioned to hold a specific component. The layout of these components can be seen in Figure 3.10. It was also important to mention that the width of each component section is equal to the width of the component leaving no empty spacing between the component exterior surface and the interior surface of the powder spray device shell.

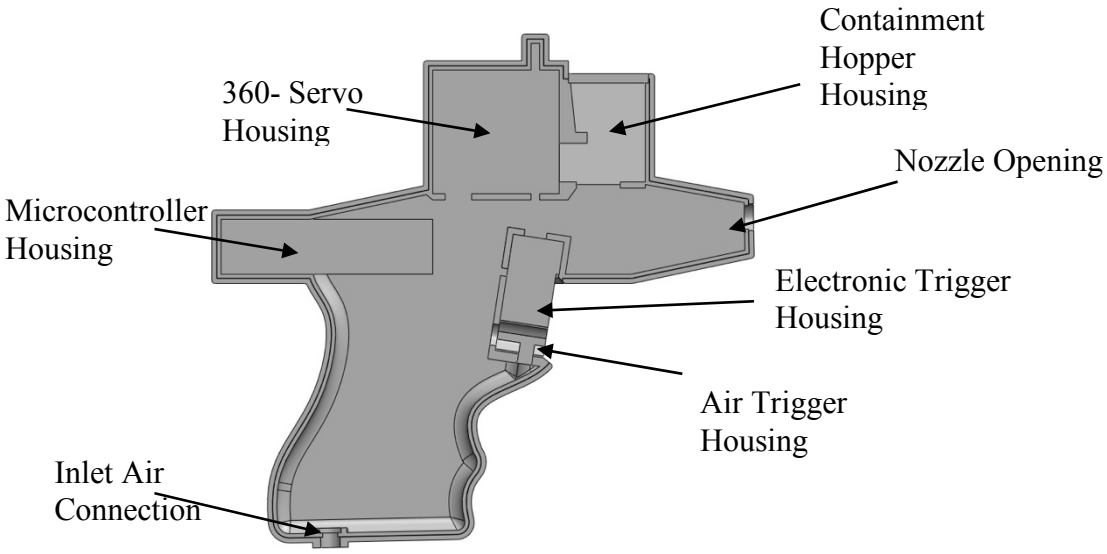

Figure 3.10. Internal component schematic for device shell

3.1.5. Air Source

Functionality of the powder spray device depends heavily on the flow of pressurized air. The source of air must meet a set of requirements which will lead to ideal device performance. These requirements include a continuous, clean, and adjustable supply of air to the powder spray device. The source of air used for the duration of this project was Master Airbrush professional high performance single-piston air brush air compressor, Figure 3.11.

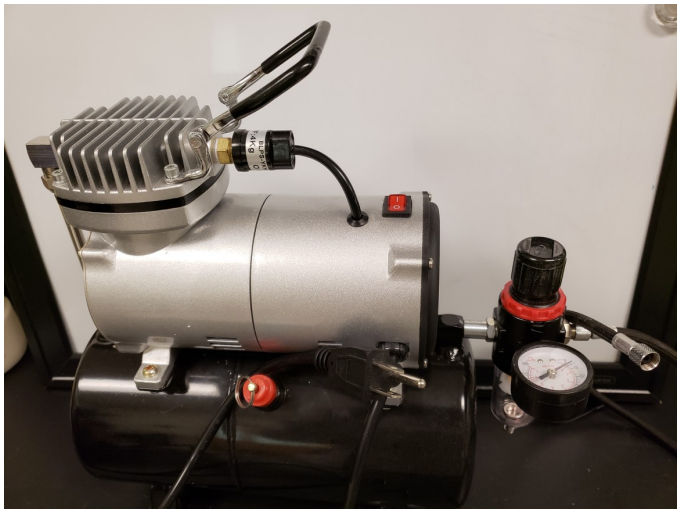

Figure 3.11. Master Airbrush Model TC-20T – Professional High Performance Single-Piston Air Brush Air Compressor with Air Storage Tank, Regulator, Gauge & Water Trap Filter.

The TC-20T air compressor was chosen because it meets all requirements. Designed to produce full-capacity air on demand capable of delivering an air flow of 25 ltrs/min . Dual tanks allow for zero pulsation as air exits through the larger tank. This tank is fed via the smaller tank isolating the exiting air flow from the compressor and any associated pressure fluctuations. The TC-20T has a water trap filter which filters

water and other impurities out of the air before leaving the compressor. This will provide clean air and prevent moisture from causing particle agglomeration or even condensation on the interior walls of the device tubing. A diaphragm pressure regulator with gauge is available to accurately manipulate the output pressure. The exit threading is 1/8'' bsp.

3.1.6. Switch Controls

The spray device was designed to be manually operated via a conventional trigger system. To operate both the electronic components as well as the flow of air at the same time two triggers were used. The electronic switch used for this prototype was a commonly used micro switch model KW11-7-1, Figure 3.12. The wiring diagram for this component is presented in section 3.1.9. By introducing a voltage to the normally open terminal, the trigger circuit will be completed only when the trigger is engaged. This directs the flow of electricity to the common terminal and then towards the microcontroller where the signal is registered as an input and then acted upon. Another appealing attribute was that the trigger extends past the body of the switch. Meaning that this trigger can be used to operate more than one switch if necessary.

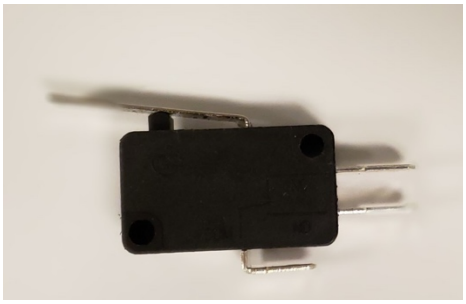

Figure 3.12. Micro-Switch KW11-7-1.

The air trigger used was a push button style manually operated air switch that is light weight, simple and compact. The air switch can be seen on the right-hand side of Figure 3.13. This switch was pulled from an existing Master Airbrush model G70 seen on the left-hand side of Figure 3.13. This push style switch can be activated in harmony with the electronic switch. Seen in Figure 3.22, the electronic switch trigger overhangs

and can be used to simultaneously activate the air trigger. Air enters the air switch from the side opposite the push button and exits perpendicular via a port located on the edge. The inner diameter tubing size used to bring air from the compressor to the air switch is 3.2 mm, the inner diameter of the tubing that carries air away from the air switch is 1.6 mm.

Figure 3.13. Master Airbrush Model G70 (Left). Trigger mechanism from G70 (Right).

3.1.7. Vibrational Motors

Fluidization of the powder was induced by means of two small compact vibrational motors. These motors, Figure 3.14, are extremely light and compact. Weighing only 0.9 grams, each motor is capable of an output of ~83 Hz at 5 V. The motor operates on an interval anywhere from 2-5 V. Having a thickness of only 2.7 mm, this motor unit was easily incorporated within the device shell without having to drastically modify existing geometries. At 5 V, only 100 mA of current is drawn by the vibrational motor which makes this source of vibration energy a good candidate for a battery powered device.

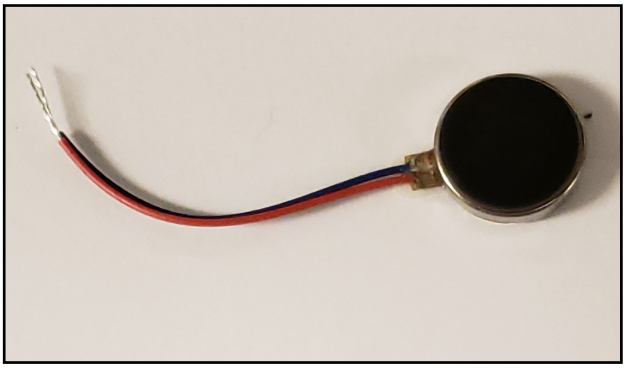

Figure 3.14. Vibrating mini motor disk from adafruit.

3.1.8. Rotary Valve

An advantageous component to incorporate within the powder spray device was one capable of mediating or controlling the flow of powder as it travels down the dosing chute. The addition of such component is investigated.

The decision to abandon a pinch valve mediated dosing mechanism was a result of much deliberation. There are a few key issues surrounding the media-isolation (pinch) valve which deem it undesirable for this device. One issue was related to the size and weight of the component. A media isolation valve was much larger and heavier than an average servo motor. This valve also operates on the concept of pinching the outer surface of tubing until the inner surface comes into contact with itself, effectively stopping the flow of material. The issue with this was related to the effect pinching may have on a powder. For certain powders, pinching may result in a compacted agglomeration of particles impeding flow and clogging the device. Furthermore, the isolation valve required an input voltage of 12 V for operation. This is a high input value which required electronic circuitry to enable control of a 12 V valve while using an Arduino microcontroller capable of a maximum output voltage of only 5 V. The electrical schematic for the pinch valve circuit can be seen in the appendices section 5.1.

The decision made was to substitute a servo motor for the media isolation valve. The servo motor chosen for this application was the Parallax HighSpeed 360 servo,

Figure 3.15. This servo was unique in that it was capable of rotating a full 360° continuously, conventional servos offer only 180° of rotation. The 360° servo had the ability to rotate up to 120 rpm and is capable of operating at the 5V output limit of the Arduino. This servo was used to operate a rotating dosing shaft which will make up the rotary valve.

Figure 3.15. Parallax Incorporated High Speed 360 Feedback Servo motor.

The rotating dosing shaft was designed using SolidWorks CAD software and prototyped via 3-D printing with ABS plastic. The resulting component can be seen in Figure 3.16, where one end of the shaft was fit with a gear designed to fit onto the gear of the 360° servo, Figure 3.17. This dosing shaft was inserted into the containment hopper and serves as a rotary valve. Due to tolerance limitations associated with 3-D printing, air leakage through the dosing shaft was an immediate issue. A layer of clear

nail polish coat was applied to the surface and an O-ring was used to seal the connection. This alleviated the issue of air leaking.

Figure 3.16. O-Ring to prevent air leak (Left). Parallax 360° Servo gear connection with rotating dosing shaft (Right).

Figure 3.17. Gear design on rotating dosing shaft.

Two design variations were considered for the rotary valve. Seen in Figure 3.18., quad chamber and a canal geometry were each drawn using SolidWorks CAD software. The quad chamber was designed such that one chamber fills with powder while one was being emptied. Rotating the quad chamber geometry allows for an even and relatively continuous dose each rotation. The canal geometry was designed to open the dosing chute for an instant allowing the free flow of material. The canal design essentially drops a slug of material into the mixing chamber each rotation. The servo motor can be programmed such that the canal is exposed for a predetermined set of time, controlling the release of powder.

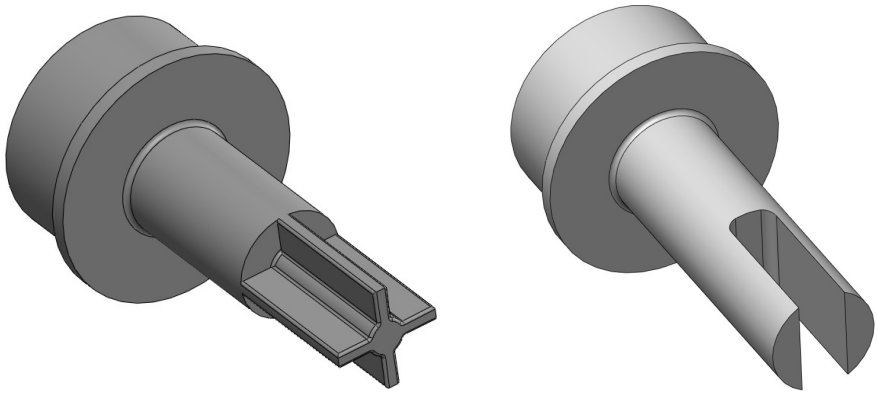

Figure 3.18. Quad chamber rotating dosing shaft (Left). Canal geometry dosing chamber (Right).

After trial testing was conducted using both variations of the rotary valve, it became clear that there were some inhibiting factors interfering with the performance of this component. A major issue related to the strength of 3-D printed ABS. Due to the size of this rotating dosing shaft, failure was extremely common. Furthermore, the tolerance between the rotating dosing shaft and its exterior surrounding was variable

and significant. This would allow for powder to leak into the shaft and interfere with or even halt the rotary valve. Furthermore, the addition of the rotary valve seemed to increase (for some powders) the formation of cohesive arches and actually prevent the flow of powder. This could be due to the geometric restraints associated with the prototyping process. It could also be due to improper geometry or sizing of the rotary valve. Further design and consideration was needed to improve the rotary valve performance. High quality prototyping and better tolerance is needed to properly integrate this component with the powder spray device. For the reasons mentioned, the rotary valve component was abandoned for the scope of this project.

3.1.9. Electronic Integration

Once all of the components needed for the spray device are decided upon, it was necessary to integrate them with each other so that each individual performance can be linked. As mentioned in section 2.1, all soldering was done in a secure and safe area designed to eliminate any harmful vapors.

An Arduino RoboRed was used as the microcontroller due to its ability for tailored output voltages as well as simplicity in component control. The goal was to control each individual component via one input. This input will come in the form of an electronic switch as the trigger is pulled by the user. A complete powder spray device electrical schematic can be seen in Figure 3.19. Here the normally open (NO) terminal of the switch is connected to the high voltage supply for the circuit. Only when the trigger is activated will the normally open terminal be connected with the common terminal. When this happens, an electrical signal flows from the NO terminal to the COM terminal. The common terminal was connected to an input pin and ground. Any time a signal passes through the COM terminal (anytime the trigger is pulled) the D2 pin of the Arduino reads an input signal. Arduino was coded to recognize this signal and then turn on other components while this signal is active. In other terms, all components are activated when the trigger is pulled. The vibrational motors are controlled via NPN transistors. When a signal is sent from the Arduino it reaches the base terminal of the NPN transistor. This allows current to flow freely from the

collector to the emitter. The free flow of current through the motors causes them to produce vibrational energy.

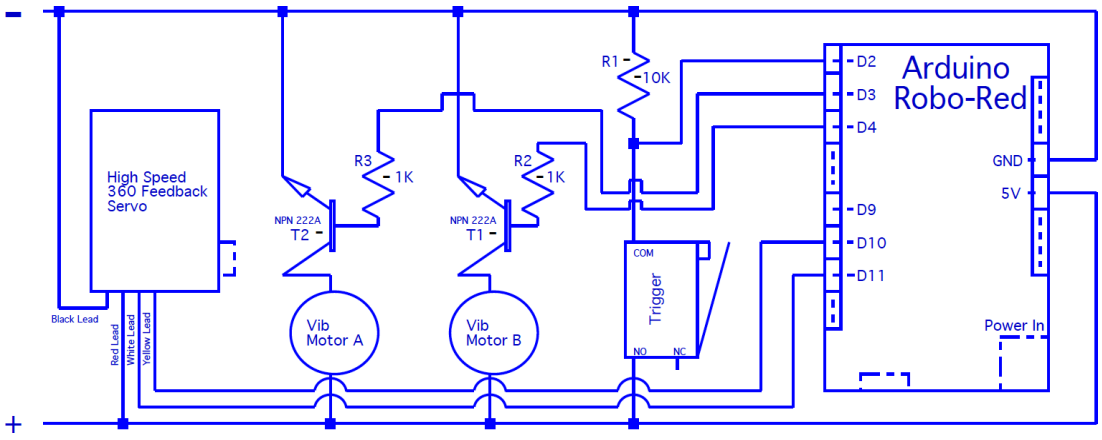

Figure 3.19. Electronic schematic of Powder Spray Device circuitry. Two vibrational motors, a trigger switch, a high speed 360-Servo and an Arduino RoboRed are needed to complete the circuit. Powdered by a 12 V 1 A wally wort, the built-in Arduino voltage step down circuitry will provide up to 5 V to each component.

After the circuit was drawn and each component was connected in accordance with their data sheets a prototype circuit can be assembled. Initial circuit prototypes worked as intended, however from an organizational perspective they were hardly up to standard. The disarray of electronic components can be seen in Figure 3.20 (Left). After the wiring schematic was finalized, a more compact electric circuit was prototyped. This compact circuit can be seen in Figure 3.20 (Right). Here all wiring, resistors and transistors were hidden under a Perma-Pro small mint tin size breadboard PCB from Adafruit. The only exposed circuitry was that which pertains to the vibrational motors, switch or the 360-Servo. This compact circuit fits into the spray device shell concealing the electronics from any exterior conditions.

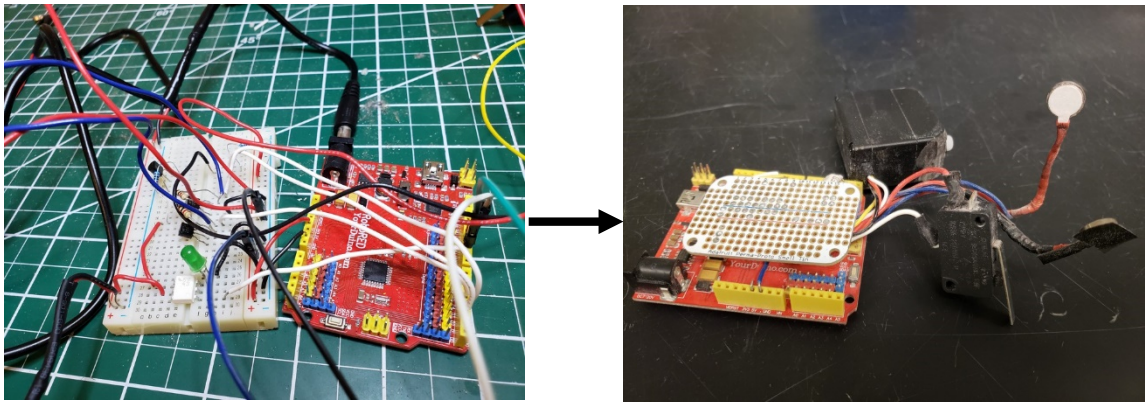

Figure 3.20. Consolidation of electronic components (Left to Right). Important so that all components can fit conveniently in the device shell isolated from environmental hazards.

3.1.10. Complete Device Prototype

With the component selection and custom design aspects of prototyping complete, all elements of the powder spray device must come together in one system. A look at the completed prototype including the storage mechanism can be seen in Figure 3.21. Notice how the trigger mechanism, when pulled, activates both the air and electronic controls. This made for an easy and simple user experience. The storage mechanism was attached to the containment hopper and sits vertically as in the conceptual gravity fed design.

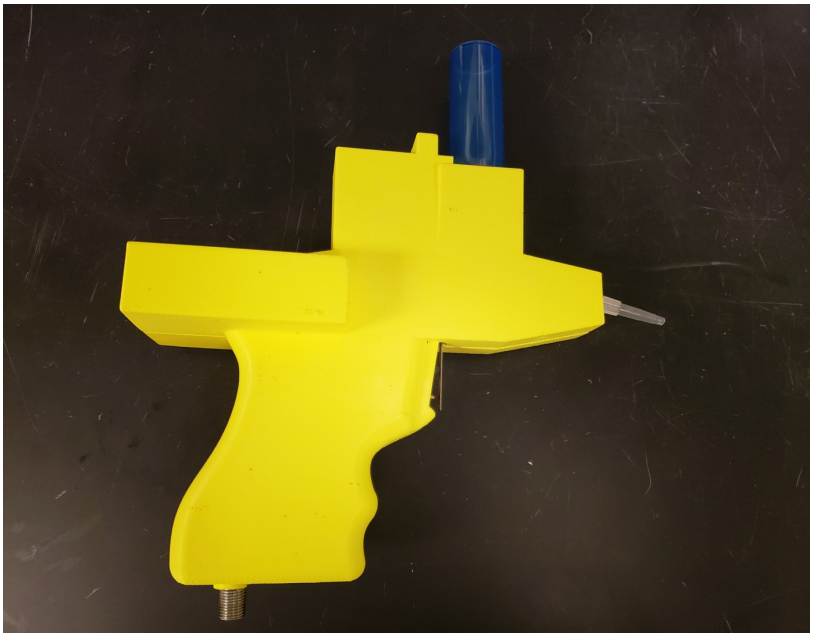

Figure 3.21. Complete prototype of powder

Figure 3.22. Complete spray device interior component split view.

The interior component layout can be seen in Figure 3.22. Air enters through the base of the handle via a 1/8'' bsp connector fitting. The other end of this connector was fit with 3.2 mm inner diameter tubing which carries the compressed air to the air switch. All electronic components fit within the confines of the spray device shell. Power was introduced to the Arduino through the rear of the device shell, Figure 3.23. A conventional 120 V AC input to 12 V 1 amp DC output wally wort was used to manage power from the grid and supply the device with necessary energy requirements.

An important component added to the finalized prototype is a check valve. A check valve was added between the exit of the air switch and the inlet of the containment hopper, Figure 3.24. This prevents the backflow of air/powder mix from

getting into the air switch and clogging the push mechanism. The nozzle used was a modified 200 μL micropipette tip. The exit diameter was 2.75 mm.

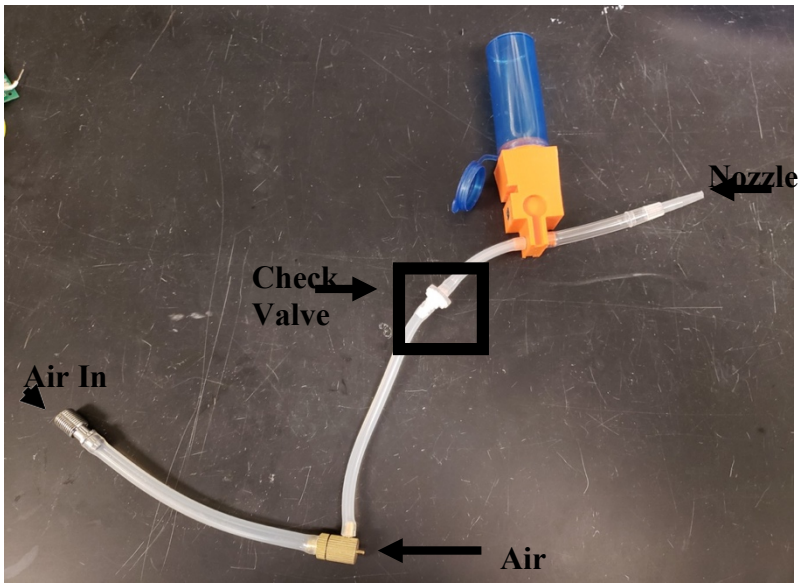

Figure 3.24. Powder spray device internal air flow path. schematic.

3.2. Scanning Electron Microscopy

Imaging of both non-biological and biological powders was done in an attempt to understand any correspondence between physical properties and flow behavior. All images have been assembled and displayed in Table 3.2. Characteristics such as homogeneity and particle size were deduced from the images. These observations were compiled in Table 3.1. Non-biological powders display a homogeneous composition while biological powders did not. This can be attributed to the manufacturing process. This characteristic does have an effect the flow characteristics however it is not a determining property as corn meal and baking powder have similar angle of repose to that of alginate, section 3.6. Furthermore, the non-homogeneous composition and flakey particles of methacrylated alginate do not interfere with ability to test for angle of repose, which is an indicator of flow behavior. These images suggest that although particle size and powder composition will affect flow properties, they are not the only factors to consider as they do not directly regulate flow.

Table 3.1. Description of visual powder characteristics. Homogeneity and particle size were tabulated for comparison and analysis.

Powder Type	Average Particle Size (μm)	Non Homogeneous	Semi Homogeneous	Homogeneous
Alginate	~ 20		✓	
ALG-GM	Flakes	✓		
ALG-GM + NaOH	Flakes	✓		
ALG-GM + KOH	Flakes	✓		
ALG-MA + NaOH	Flakes	✓		
ALG-MA + KOH	Flakes	✓		
Gelatin Powder	~ 5			✓
Baking Powder	~ 10			✓
Corn Meal	~ 10			✓

Table 3.2 Collection of SEM images for both biological and non-biolical powders.

ALG Powder

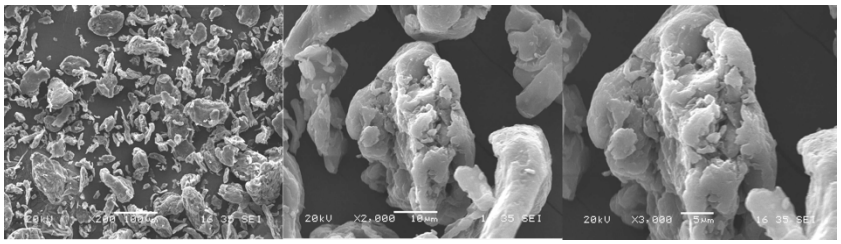

GM-ALG: Glycidyl

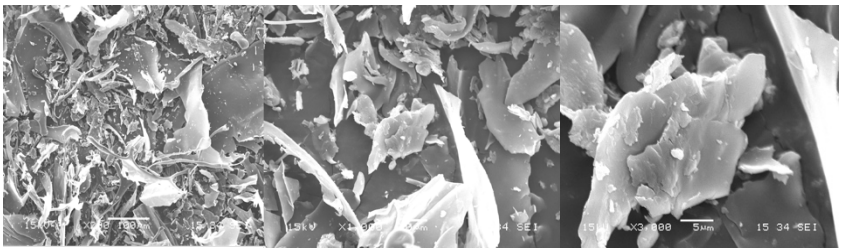

GM-ALG + NaOH

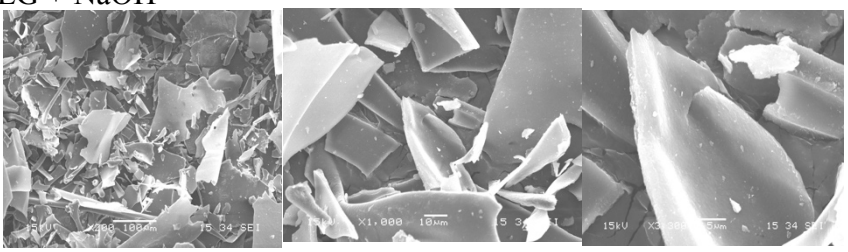

GM-ALG + KOH

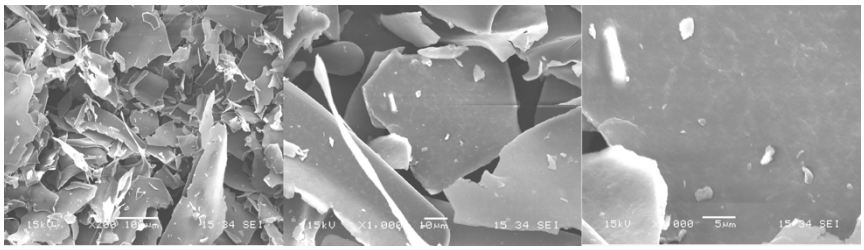

ALG-MA + NaOH

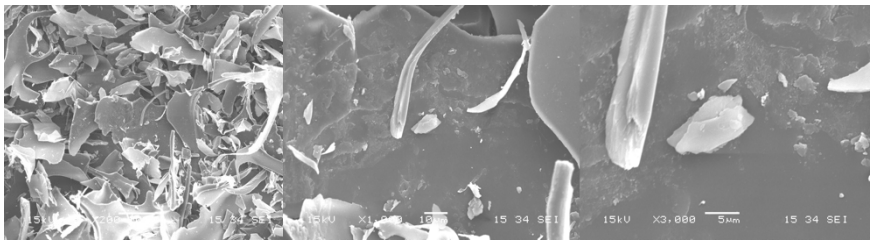

ALG-MA + KOH

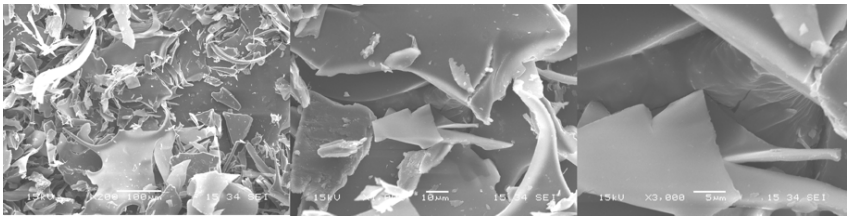

Gelatin Powder

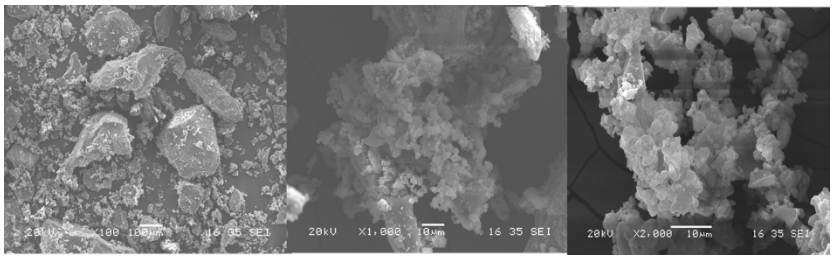

Corn Meal

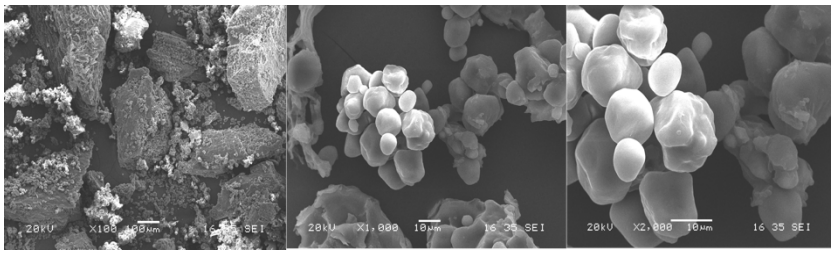

Baking Powder

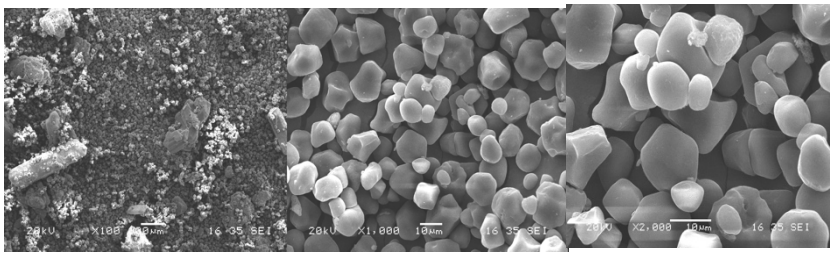

3.3. Proton Nuclear Magnetic Resonance Spectroscopy

Chemical modifications to the alginate backbone were confirmed and quantified by means of NMR spectroscopy analysis. The free induction decay (fid) was collected and passed through a Fourier transform before analysis. Figure 3.25 depicts the resulting peaks for ALG-MA chemical modifications and Figure 3.26 shows the same information for ALG-GM chemistry. Degree of modification (DOM) was calculated by comparison of the integration of peaks as a ratio of area under the peaks. This was done as an attempt to show that not only did the methacrylation chemistry take, but the addition of salts (KOH and NaOH) do not have any effect on the reaction or DOM. The DOM calculated was ~15% for ALG-MA and ~30% for ALG-GM. Glycidyl has an epoxy group which is fast reacting which is why a larger DOM is seen from the ALG-GM.

Looking at Figure 3.25 and Figure 3.26, the alginate peak corresponding to the hydrogens on the alginate backbone was shown in all spectra. Though this peak was slightly shifted after the addition of salts, this could be evidence of an ionic interaction or attraction between the alginate backbone and the Na or K ions. This shift does not affect the DOM however there is an interaction happening with the alginate backbone. This would suggest that the attempt to bring down the resultant static charge seen on ALG-MA and ALG-GM has worked by adding free ions to the solution.

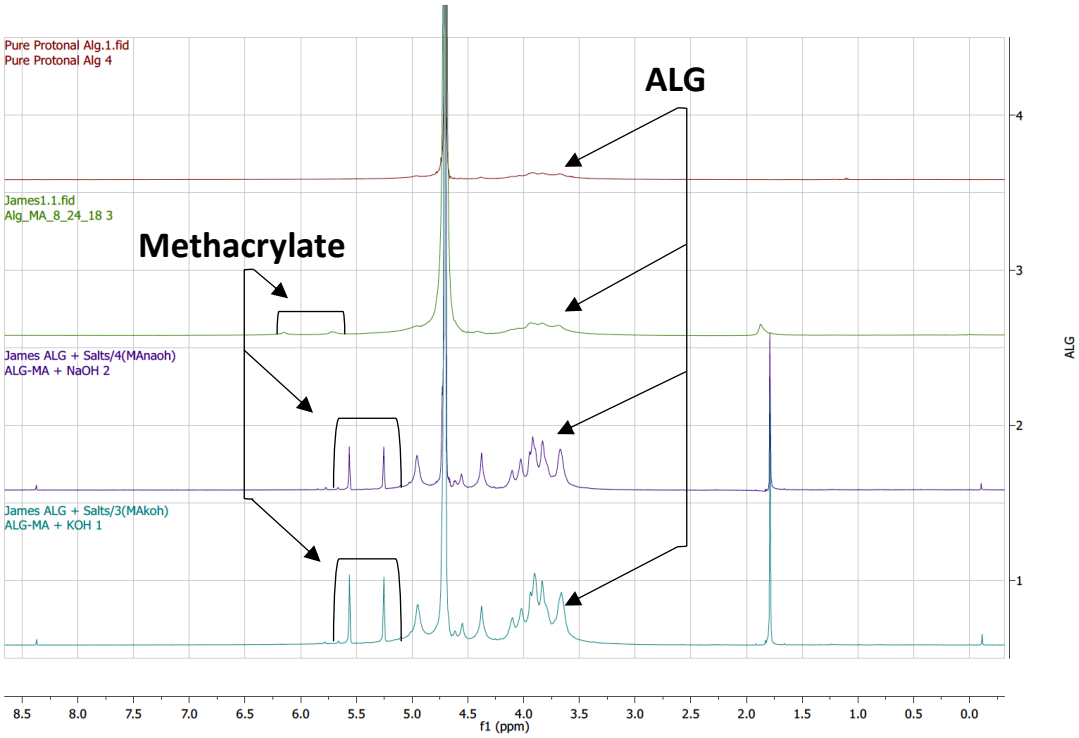

Figure 3.25. NMR spectra for ALG-MA chemistry.

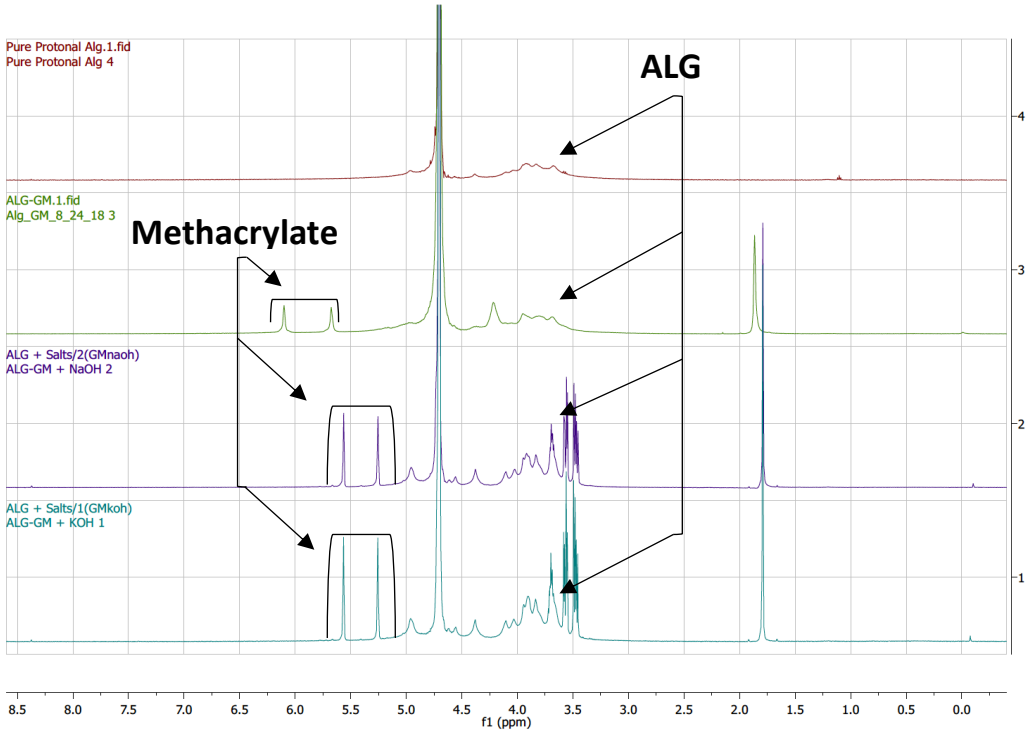

Figure 3.26. NMR spectra for ALG-GM chemistry.

3.4. Powder Manufacturing

Powders were created using a mortar and pestle. The resulting powders were generated and an example of these results can be seen in Figure 3.27. After the addition of ions in the form of salts, the material was much more compliant during powder processing. Without the addition of salts, the powdered material has an extremely high static charge as well as having long thin fibrous structure similar to that of cotton candy. The light weight ALG-MA powder has an extremely strong static charge and tends to agglomerate with other particles. This confirms that the addition of salt allows for a more favorable powder to be generated with respect to flowability and interparticle interactions.

Figure 3.27. Powder production process for ALG-GM. The top row consists of ALG-GM non powder (Left) and ALG-GM powder (Right). The bottom row shows ALG-GM+KOH non powder (Left) and ALG-GM+KOH powder (Right).

3.5. Spray Data

3.5.1. Spray Field

To better understand how the powder spray device will perform in a clinical setting, spray field data was collected using a host of powders both biological and non-biological. The powders were tested using both circular and oval containment hopper designs, Figure 3.7. The biological powder used for this test was alginate. This powder was tested at 10,20 and 30 psi. The results of this study are seen in Figure 3.28 and Figure 3.29. Both graphs suggest there was not a significant change in impact diameter with respect to device pressure. It is important to note that at a device pressure of 10 psi, both the circular and oval containment hoppers are not capable of propelling powder a full 12 cm to reach the impact surface. Therefor these data points were never tabulated. A comparison between graphs in Figure 3.29 reveals that the impact diameters are relatively similar between containment hopper geometries. Although the oval containment hopper resulted in slightly larger impact diameters, it was hypothesized this can be attributed to the increased mass of powder being sprayed. The larger dosage of powder being sprayed means there was more inertia present causing the wider diameter spread. This realization leads to the idea that impact diameter was more closely related to density and composition of the particulate being sprayed over the device pressure.

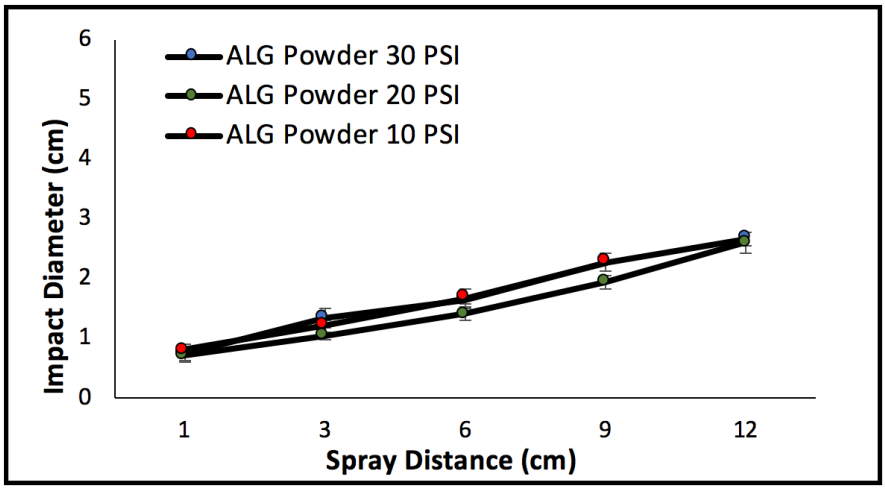

Figure 3.28. Spray field results testing alginate powder across a range of device pressures for circular containment hopper design.

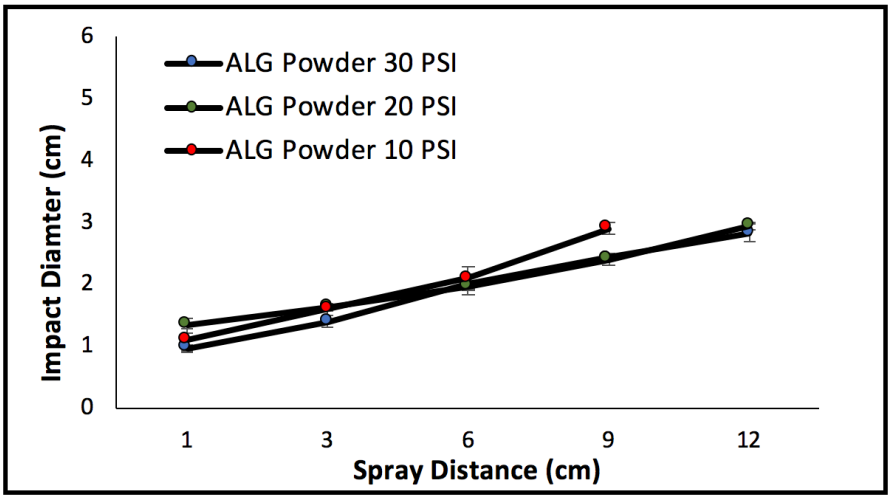

Figure 3.29. Spray field results testing alginate powder across a range of device pressures for oval containment hopper design.

Non-biological powder spray field data was collected for both containment hopper designs. As previously mentioned, there was no significant change in impact diameter with respect to device pressure and so for this reason all testing on non-biological powders was done at 30 psi. These results can be seen in Figure 3.30 and Figure 3.31. Very little variation of impact diameter was observed between different powder types, with the exception of gelatin sprayed using the circular containment hopper. This behavior could be due to experimental or environmental influences.

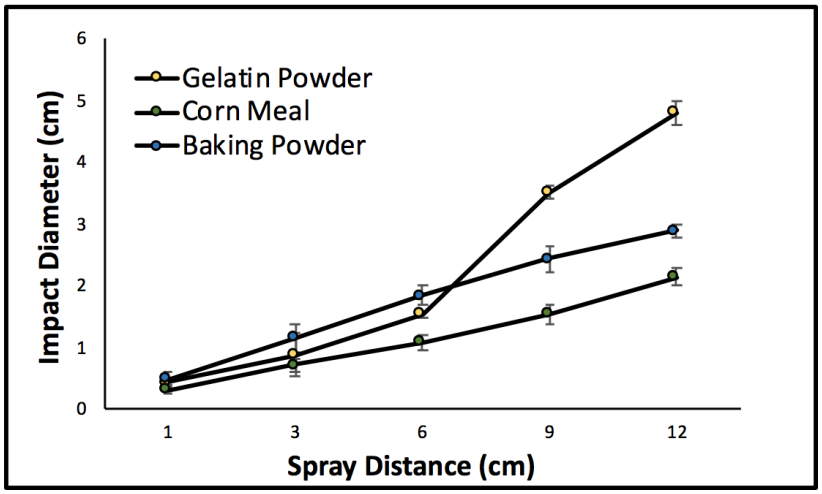

Figure 3.30. Spray field results testing non-biological powders at 30 psi for circular containment hopper design.

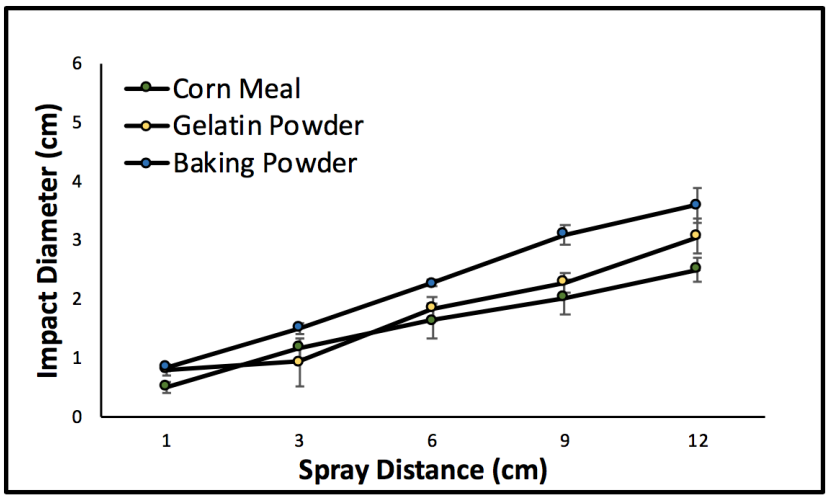

Figure 3.31. Spray field results testing non-biological powders at 30 psi for circular containment hopper design.

To extend the concept of spray field beyond the powders used during this experiment a mathematical relationship is preferred. A proportionality between distance and jet radius is presented in equation 3.1, where R is the radius of the jet and x is the downstream distance from the jet nozzle [28]. This equation does not perfectly capture behavior of the powder spray field as it was derived based on the kinetic energy dispersion of a jet as it travels further away from the nozzle. Nevertheless, this equation can be loosely applied as an approximation value for spray distances up to 6 cm. Beyond this distance it appears that particulates in the air stream dominate system behavior.

$$R = \frac{1}{5}x \tag{3.1}$$

3.5.2. Spray Rate

The rate at which powder leaves the spray device was important to describe before considering possible applications. To do this, spray rate data was collected on both biological and non-biological powders. Alginate was used as the biological powder and was tested using both circular and oval containment hoppers at 10, 20, and 30 psi. The results of this study can be seen in Figure 3.32 and Figure 3.33. Initial observation of the data suggested that device pressure has little effect on the amount of material being sprayed through time. Although, the oval containment hopper discharges nearly twice as much powder at 10 psi than at 20 psi and 30 psi. A similar trend was observed between the non-biological powders, Figure 3.35. This could be due to the larger size of the oval dosing chute in conjunction with low device pressure allowing for increased mass flow through the funnel. This phenomenon was not observed with the circular containment hopper as the mass flow rate does not change. Suggesting that there is a minimum threshold pressure with respect to each containment hopper dosing chute geometry.

One design goal of this spray device was to allow for consistent deposition of powder through time. To analyze this, each individual data set was considered. A linear relationship between mass and time indicates a consistent spray rate. The slope of each line corresponds to the mass sprayed per second for that particular powder. Although the data did not result in perfectly straight lines, the slope of best fit line can adequately describe the spray rate for a given powder. Analysis of Figure 3.32 and Figure 3.33 lead

to a calculated an average spray rate of 0.021 g/s for the circular containment hopper and 0.058 g/s for the oval containment hopper when spraying alginate powder. The oval containment hopper exhibits a larger amount of mass being sprayed after 3 seconds at 10 psi. This could be due to the larger oval dosing chute allowing too much powder to build up at low system pressure. The low pressure does not offer enough energy to keep up with the amount of powder being introduced into the air stream. Neglecting the 10 psi data set, the oval containment hopper exhibits a spray rate of 0.044 g/s. This was predicted as the cross sectional area of the oval dosing chute is roughly twice that of the circular chute .

It is important to note that these values are not absolute and there are other factors that will effect spray behavior such as powder type. Regardless, the collected data is a good measure of generalized device performance. To attain a specific spray rate, first the powder being sprayed must be decided on. Once this decision has been made, a variety of containment hopper geometries can be developed. Testing and analysis of these various geometries will demonstrate what the specific dosing chute area needs to be in order to achieve the desired spray rate.

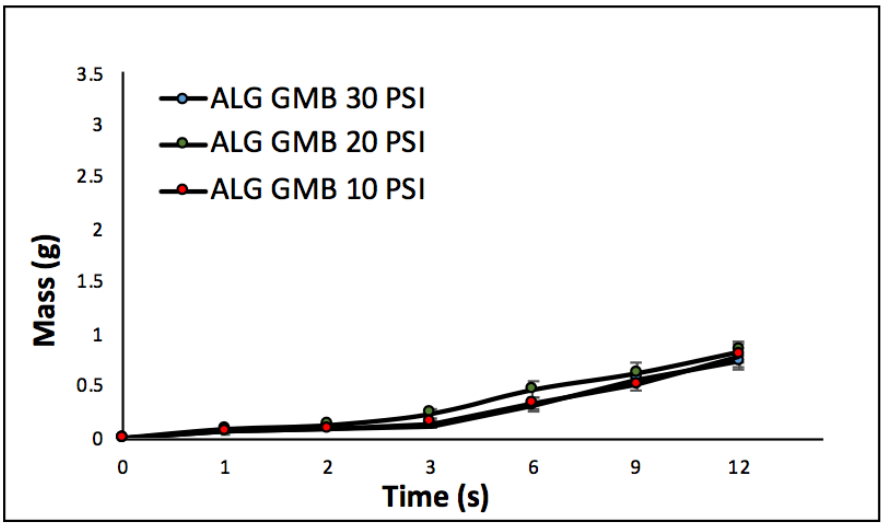

Figure 3.32. Spray rate for alginate powder across a range of pressures using circular containment hopper.

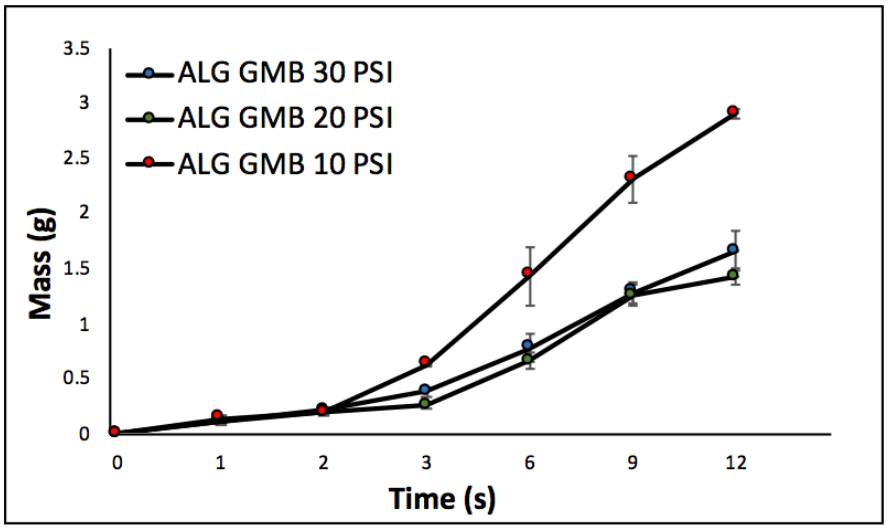

Figure 3.33. Spray rate for alginate powder across a range of pressures using oval containment hopper.

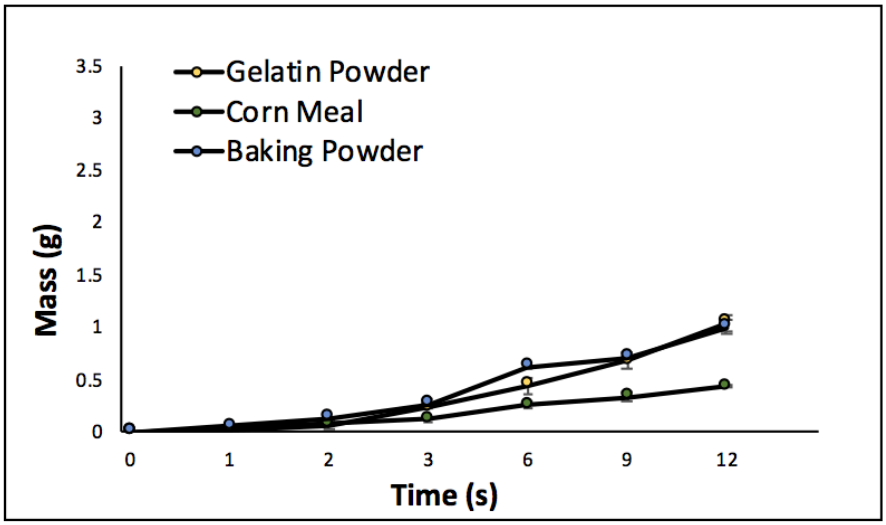

Figure 3.34. Spray rate for non-biological powders at a range of constant pressure using circular containment hopper.

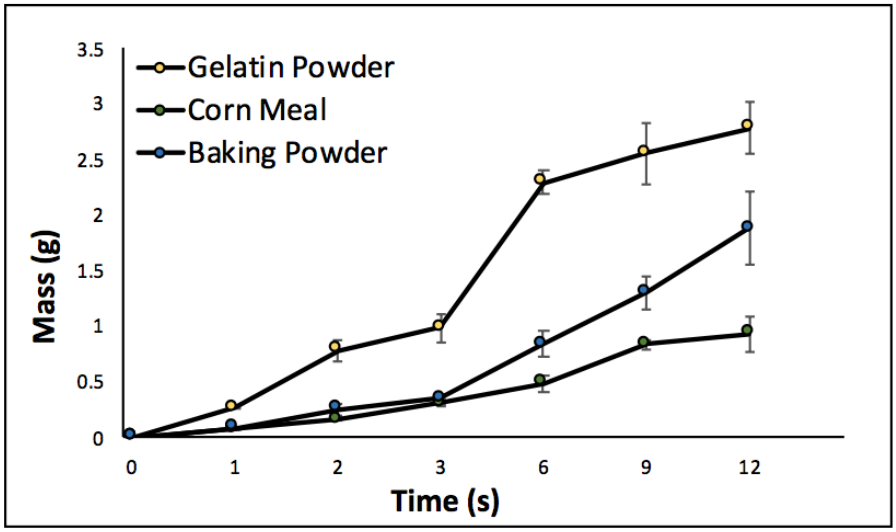

Figure 3.35. Spray rate for non-biological powders at a range of constant pressure using oval containment hopper.

3.6. Angle of Repose

To gain an understanding of how a powder might flow, the angle of repose was an easy way to generate a comparison between powders and flowability. This method of characterization is often used in industry. A table of general flow characteristics with respect to the angle of repose can be seen in Table 3.3. Here any angle above 66° will result in a powder with extremely poor flow properties. Ideally a smaller angle of repose will result in better powder flow properties.

Table 3.3. Chart quantitatively relating angle of repose to powder flow characteristics. [1]

Flow	Repose Angle (°)	Static cohesive index
Excellent	25-30	< 0.2
Good	31-35	0.3 - 0.5
Fair	36-40	0.6 – 0.8
Passable	41-45	0.9 – 1.2
Poor	46-55	1.3 – 1.7
Very poor	56-65	1.8 – 2.4
Very very poor	>66	> 2.5

All tabulated values for angle of repose can be seen in Table 3.4. In general, the powders tested displayed similar angles which suggests that each powder exhibits similar flow properties under identical conditions with a few exceptions. Synthesis of powdered methacrylate alginate (ALG-MA & ALG-GM) resulted in an angle of repose greater than 66° suggesting that this powder will not flow. Gelatin powder exhibited the smallest angle of repose while other non-biological powders exhibited passable angles. Biological powders range from an angle of repose of 47° to 55° placing them in the poor flow category. The results of this study suggest that all powders tested flow with the exception of ALG-GM and ALG-MA. This is further supported by spray data collected and discussed further in section 3.5.

Table 3.4. Chart containing experimentally collected angle of repose values for both non-biological and biological powders.

Powder	Height of Pile (mm)	Diameter of Pile (mm)	Angle of Repose (Radians)	Angle of Repose (Degrees)
Yellow Corn Meal	17	35	0.77	44
Baking Powder	16	35	0.74	42
Gelatin Powder	9	35	0.48	27
Alginate Powder	19	35	0.83	47
ALG-MA	NA	NA	NA	>66
ALG-GM	NA	NA	NA	>66
ALG-MA + KOH	23	35	0.92	53
ALG GM + KOH	20	35	0.85	49
ALG-MA + NAOH	25	35	0.96	55
ALG GM + NAOH	21	35	0.88	50

3.7. Burst Pressure

Analysis of burst pressure between ALG-MA and a powdered ALG-MA+Salt was done to determine if the powder manufacturing procedure compromises the alginate backbone interfering with the rapid polymerization crosslinking process. Graphical representation of each data set can be seen in Figure 3.36 and Figure 3.37. The control used for this study was the data representing ALG-MA (non-powder). The results of this testing confirmed that ALG-MA exhibited burst pressures ranging from 35 inH2O up to 65 inH2O. The average burst pressure for the non-powdered samples was 77.81 mmHg (41.6 inH2O) with a standard deviation of 37.73 mmHg. This range can be attributed to inconsistencies in test sample thickness. Overall, data confirmed that non-power ALG-MA properties are suited for further investigation into the application of this material as a tissue sealant.

The results obtained by testing a powdered ALG-MA+Salts suggest otherwise. Seen in Figure 3.37, the powdered material was simply unable to perform demonstrating no burst pressure capability. The average burst pressure 2.25 mmHg (1.2 inH2O) with a standard deviation of 1.42 mmHg. This confirms that the powder manufacturing procedure compromised the alginate backbone inhibiting the ability to crosslink. The physical cause of this can be attributed to shortening of polymer chains or interference of salt ions with the polymerization process. Continued testing and chemical alteration is needed in order to confirm and describe the root cause of this phenomenon. Although the addition of salts to the material solution allows for a better

powder consistency, Figure 3.27, the effect on material performance negates the application of this powder production method for future studies.

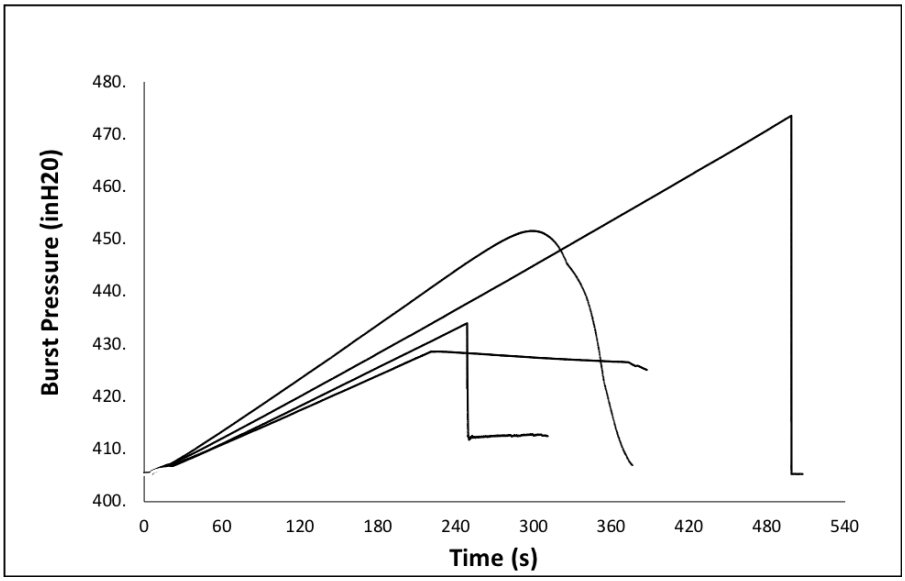

Figure 3.36. Burst pressure for non-powder ALG-MA.

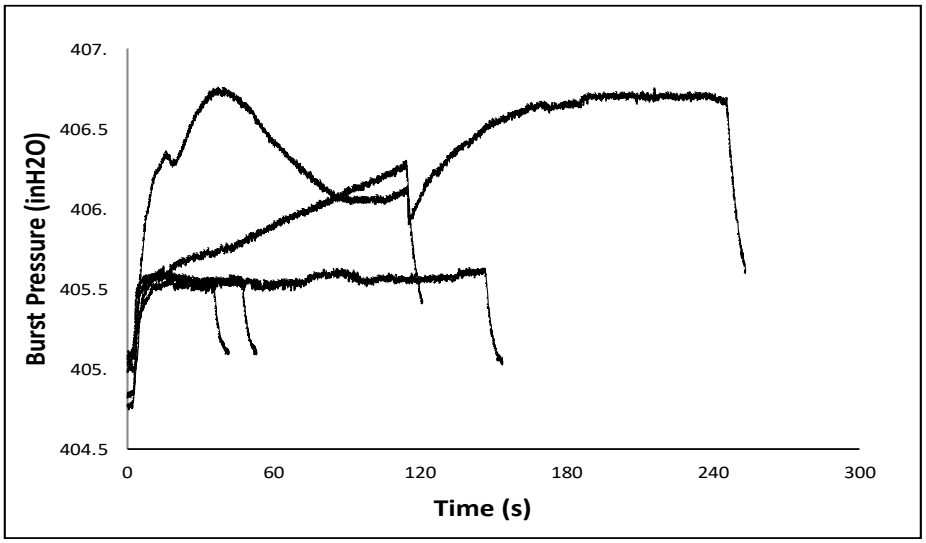

Figure 3.37. Burst pressure for powder ALG-MA.

3.8. Efficacy of Clinical Application

An ex-vivo experiment resulted in the successful deposition of alginate powder onto a porcine heart by means of the powder spray device. Alginate powder was then ionically crosslinked with a calcium chloride solution to elicit hydrogel formation. The hydrogel coating can act as a sealant and be used to deliver drugs or other forms of therapeutics. The powder spray device method for application was suitable for controlled deposition in-vivo. Continued testing is needed to explore other areas of application.

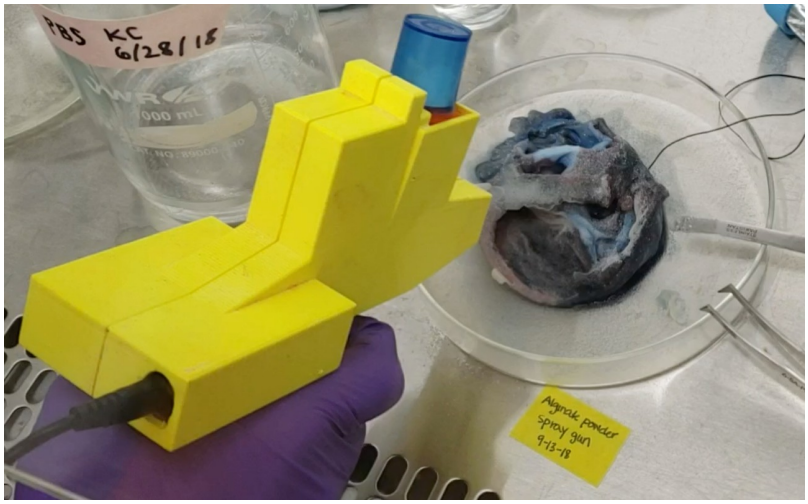

Figure 3.38. *Ex-vivo* experiment testing efficacy of powder spray device. Successful deposition of powder suggests further testing related to clinical application.

CHAPTER 4: CONCLUSOINS

Research on the application method of biological powders was investigated. The objective of this research was to strengthen powder sealant technology with a reliable application method. Our novel device was applicable for the controlled spraying of dehydrated powder particulates of a variety of compositions, shapes and sizes. System design and prototyping was completed and the device analyzed for efficacy. Spray field and spray rate were collected for a variety of powders as well as over a range of pressures. The device demonstrated consistency during operation and was capable of handling powders of varying compositional makeup. Spray rate and spray field data was collected in an attempt to quantify the device performance. A generic mathematical proportionality was established between spray distance and impact diameter to describe spray field. An average spray rate was defined for alginate powder. Angle of repose predicted that all powders exhibit flow capabilities except for the ALG-GM and ALG- MA powders. Burst pressure analysis concluded that the process used for powder formulation had a damaging effect on chemical structure, negating this method of powder production to be used for the development of tissue sealants.

An ex-vivo experiment resulted in successful spraying of alginate powder on a porcine heart. Suggesting that this technology is a versatile delivery method which has a wide variety of medical applications. Powder sealant can be used to cover suture lines and prevent leakage along the suture site. Furthermore, the sealant would behave as a physical barrier stopping bacteria from entering the wound site. Additionally, the

applications extend outside of the medical arena and into other large industries such as food and cosmetics. The multiuse functionality of the proposed device could have profound influence both in and out of the medical community. The unique yet simple design of the spray device may enhance innovation of the dry powder sealant class. Technology may be able to be licensed on its own, with applications outside of the medical field.

Looking forward, future design iterations will include continued prototyping of device components. Containment hopper modules can be developed specifically to induce a greater venturi effect by introducing air through a convergent channel prior to where the air stream comes into contact with powder. This may help with better device performance at low system pressures. To attain a homogenous suspension of powder in the air stream, a swirling flow is desired. To accomplish this, fins can be added to the interior walls of the convergent channel to induce swirling prior to coming into contact with powder. For convenience, a portable version of the spray device must be explored. This would include a smaller microcontroller powered by batteries. A compressed air cannister must be included to provide sterile air on the go as needed. To regulate the amount of air leaving the canister, a small adjustable pressure regulator must also be explored. For easy sterilization, all custom components must be injection molded using plastics such as polypropylene or Teflon® which can withstand high pressure and heat.

CHAPTER 5: REFERENCES

1. Automated repose angle and cohesive index measurements.
2. Carson, J.W. and B.H. Pittenger, Bulk Properties of Powders. 2013.
3. Mehos, G., Hopper Design Principles. 2016.
4. Klinzing, G.E., Dilute-Phase Pneumatic Conveying. HANDBOOK of FLUIDIZATION and, 2003.
5. Bhatia, A., Pneumatic Converying Systems.
6. Lobato, J.C.M., Conical Hopper Design for Mass Flow - Case of Study for Red Mud Powder 2014
7. Çağli, A.S., et al. Flow property measurement using Jenike shear cell for 7 different bulk solids. in Proceedings of European Congress of Chemical Engineering (ECCE-6), Copenhagen. 2007.
8. Pan, R., Material properties and flow modes in pneumatic conveying. Powder technology, 1999. 104(2): p. 157-163.
9. Fertah, M., et al., Extraction and characterization of sodium alginate from Moroccan Laminaria digitata brown seaweed. Arabian Journal of Chemistry, 2017. 10: p. S3707-S3714.
10. Muthu, C., et al., Medicinal plants used by traditional healers in Kancheepuram District of Tamil Nadu, India. Journal of Ethnobiology and ethnomedicine, 2006. 2(1): p. 43.
11. Varela, G., et al., Estimating hospital costs attributable to prolonged air leak in pulmonary lobectomy. European journal of cardio-thoracic surgery, 2005: p. 329-333.
12. Sun, J. and H. Tan, Alginate-based biomaterials for regenerative medicine applications. Materials, 2013. 6(4): p. 1285-1309.
13. Ergil, K., Chinese Herbal Medicines. Western Journal of Medicine, 2002(176.4): p. 275-279.
14. Secretariat, Traditional Medicine World Health Organization 2003
15. Bustamante-Balén, M. and G. Plumé, Role of hemostatic powders in the endoscopic management of gastrointestinal bleeding. World journal of gastrointestinal pathophysiology, 2014. 5(3): p. 284.
16. Prei, J.C., et al., Endoclot polysaccharide hemostatic system in nonvariceal gastrointestinal bleeding: results of a prospective multicenter observational pilot study. Journal of clinical gastroenterology, 2016. 50(10): p. e95-e100.
17. Telko, M.J. and A.J. Hickey, Dry powder inhaler formulation. Respiratory care, 2005. 50(9): p. 1209-1227.
18. Atkins, P.J., Dry powder inhalers: an overview. Respiratory Care, 2005. 50(10): p. 1304-1312.
19. Charron, P.N., et al., Mechanical properties and failure analysis of visible light crosslinked alginate-based tissue sealants. Journal of the mechanical behavior of biomedical materials, 2016. 59: p. 314-321.
20. Fenn, S.L., P.N. Charron, and R.A. Oldinski, Anticancer Therapeutic Alginate-Based Tissue Sealants for Lung Repair. ACS Applied Materials & Interfaces, 2017. 9(28): p. 23409-23419.

21. Chee, S.-Y., P.-K. Wong, and C.-L. Wong, Extraction and characterisation of alginate from brown seaweeds (Fucales, Phaeophyceae) collected from Port Dickson, Peninsular Malaysia. Journal of applied phycology, 2011. 23(2): p. 191-196.
22. Kühbeck, D., et al., Evaluation of the nitroaldol reaction in the presence of metal ion-crosslinked alginates. New Journal of Chemistry, 2015. 39(3): p. 2306-2315.
23. Wadell, H., Sphericity and roundness of rock particles. The Journal of Geology, 1933. 41(3): p. 310-331.
24. Ganesan, V., K.A. Rosentrater, and K. Muthukumarappan, Flowability and handling characteristics of bulk solids and powders–a review with implications for DDGS. biosystems engineering, 2008. 101(4): p. 425-435.
25. Valverde, J., A. Castellanos, and M. Quintanilla, Effect of vibration on the stability of a gas-fluidized bed of fine powder. Physical Review E, 2001. 64(2): p. 021302.
26. Ahuja, S. and S. Scypinski, Handbook of modern pharmaceutical analysis. Vol. 10. 2010: Academic press.
27. Charron, P.N., Burst Pressure Properties and Ex Vivo Analysis of Alginate-Based Hydrogels for Tissue Sealant Applications. 2015.
28. Horn, G., and M. W. Thring. "Angle of spread of free jets." Nature 178.4526 (1956): 205.

CHAPTER 6: APPENDICES

6.1. Pinch Valve Circuit